Title

Metabolically driven maturation of human-induced-pluripotent-stem-cell-derived cardiac microtissues on microfluidic chips

Journal

Nature Biomedical Engineering, 6(4)

ISSN

2157-846X

Authors

Huebsch, Nathaniel
Charrez, Berenice
Neiman, Gabriel
et al.

Publication Date

2022-04-01

DOI

10.1038/s41551-022-00884-4

Peer reviewed

Published in final edited form as:

Nat Biomed Eng. 2022 April ; 6(4): 372–388. doi:10.1038/s41551-022-00884-4.

Metabolically driven maturation of human induced pluripotent stem cell derived cardiac microphysiological systems

Nathaniel Huebsch[1,&,+], **Berenice Charrez**[1,&], **Gabriel Neiman**[1], **Brian Siemons**[1], **Steven C. Boggess**[2], **Samuel Wall**[3], **Verena Charwat**[1], **Karoline H. Jæger**[3], **David Cleres**[1], **Åshild Telle**[3], **Felipe T. Lee-Montiel**[1], **Nicholas C. Jeffreys**[1], **Nikhil Deveshwar**[1], **Andrew G. Edwards**[4], **Jonathan Serrano**[5], **Matija Snuderl**[5], **Andreas Stahl**[6], **Aslak Tveito**[3], **Evan W. Miller**[2,7,8], **Kevin E. Healy**[1,9,*]

[1]Department of Bioengineering and California Institute for Quantitative Biosciences (QB3), University of California at Berkeley, Berkeley, California 94720, USA

[2]Department of Chemistry, University of California at Berkeley, Berkeley, California 94720, USA

[3]Simula Research Laboratory, 1325 Oslo, Norway

[4]Department of Pharmacology, School of Medicine, University of California, Davis, Davis, CA 95616, USA

[5]Department of Pathology, New York University Langone Health and Medical School, New York, NY, 10016, USA

[*]**Correspondence and requests for materials** should be addressed to, kehealy@berkeley.edu.

[&]These authors contributed equally

[+]Present address: Department of Biomedical Engineering, The Washington University in Saint Louis, Saint Louis, Missouri, 63130, USA

Author contributions

N.H., B.C., G.N., A.G.E. and K.E.H. designed experimental studies. N.H., B.C., G.N., B.S., S.C.B., V.C., F.T.L-M., N.C.J. and N.D. performed experimental studies and iPSC cultures. S.W., K.H.J. and A.T. designed and executed computational modelling studies to predict molecular changes in voltage and calcium handling underlying MM-induced physiology changes. J.S. and M.S. designed and assisted in gene expression analysis studies. K.E.H., A.G.E. and S.W. guided drug-probe based studies on cardiomyocyte electrophysiology and calcium handling in MPS. E.W.M. and S.C.B. synthesized BeRST-1 dye for action potential analysis. A.S. advised on cell metabolism. K.E.H., N.H., A.G.E., and B.C. wrote the paper. K.E.H. supervised and funded the research.

Outlook

This section, or the last paragraph of the discussion if this section is not included, should only discuss the implications of the findings rather than be a repetition of findings already discussed.

Avoid hype, empty and fancy words, and overstatements. An example: ‘This overarching framework solely utilizes common standards, expediting unprecedented and unparalleled applicability opportunities’.

Methods

This section should not contain figures or tables, and should be structured in sub-sections, with appropriate specific headings such as Study design, Cell culture, Materials, Device fabrication, and Statistical analyses. The last subheading should be **Reporting Summary**. Any supplementary methods, discussion, figures and tables should be included as SI.

Reporting Summary.

Further information on research design is available in the Nature Research Reporting Summary linked to this article.

Code availability

MPS and monolayer physiology were analysed with an open source motion tracking software available for download at huebschlab.wustl.edu. Calcium transients, action potential waveforms and sarcomere regularity were analysed with in-house code that is available upon request from the authors.

Supplementary information The online version contains supplementary material available at https://doi.org/10.1038/s41551-01X-XXXX-X.

Peer review information *Nature Biomedical Engineering* thanks Reviewer and the other, anonymous, reviewer(s) for their contribution to the peer review of this work. Peer reviewer reports are available.

[6]Department of Nutritional Sciences and Toxicology, University of California at Berkeley, Berkeley, California 94720, USA

[7]Department of Molecular and Cell Biology, University of California at Berkeley, Berkeley, California, 94720, USA

[8]Helen Wills Neuroscience Institute, University of California, Berkeley, Berkeley, California, 94720, USA

[9]Department of Materials Science and Engineering, University of California at Berkeley, Berkeley, California 94720, USA

Abstract

The immature physiology of cardiomyocytes derived from human induced pluripotent stem cells (hiPSCs) limits their utility for drug screening and disease modelling. Here, we show that suitable combinations of mechanical stimuli and metabolic cues can enhance the maturation of hiPSC-derived cardiomyocytes, and that the maturation-inducing cues have phenotype-dependent effects on the cells' action-potential morphology and calcium handling. By using microfluidic chips that enhanced the alignment and extracellular-matrix production of cardiac microtissues derived from genetically distinct sources of hiPSC-derived cardiomyocytes, we identified fatty-acid-enriched maturation media that improved the cells' mitochondrial structure and calcium handling, and observed divergent cell-source-dependent effects on action-potential duration (APD). Specifically, in the presence of maturation media, tissues with abnormally prolonged APDs exhibited shorter APDs, and tissues with aberrantly short APDs displayed prolonged APDs. Regardless of cell source, tissue maturation reduced variabilities in spontaneous beat rate and in APD, and led to converging cell phenotypes (with APDs within the 300–450-ms range characteristic of human left ventricular cardiomyocytes) that improved the modelling of the effects of pro-arrhythmic drugs on cardiac tissue.

One-sentence editorial summary (to appear right below the title of your Article on the journal's website):

The metabolically driven maturation of geometrically aligned human cardiac microtissues on a microfabricated chip reduces cell-phenotype-dependent variabilities in the action-potential morphology and calcium handling of the cardiomyocytes.

Human induced pluripotent stem cell (hiPSC) technology provides an exciting opportunity for disease modeling and drug discovery. An immediate goal for cardiac tissue models formed from hiPSC-derived cardiomyocytes (hiPSC-CM) is to reduce and refine the use of animal testing in the drug development pipeline[1]. Inherent differences between species have historically diminished the ability of animal models to prognosticate drug safety and efficacy. Microphysiological systems (MPS), or organ-chips, combine 3D-architecture of tissue microenvironments with the ability to interrogate key physiological functions (for example, cardiomyocyte action potential) and well-defined delivery profiles for nutrients.

A challenge with using hiPSC-CM to predict drug safety and efficacy is the immaturity of these cells[2]. In particular, hiPSC-CM exhibit automaticity (spontaneous beating without

electrical stimulation[2,3]). Likewise, many studies report immature action potentials in hiPSC-CM. However, there is divergence in the literature in terms of whether action potential duration (APD) is prolonged or shortened in hiPSC-CM as compared to the 300–450msec directly measured in primary human adult left-ventricular cardiomyocytes[4]. Some reports indicate *prolonged* action potential duration (APD) in hiPSC-CM (ranging to over 700msec[3,5]) whereas other studies report *shorter* APD[6,7] in these cells. Importantly, "healthy" iPSC derived from individuals without known disease or disease-associated gene variants have shown large dispersion in APD[8]. All these data are in contrast to the relatively narrow APD range of 300–450msec directly measured by patch-clamp of primary human adult left-ventricular cardiomyocytes[3,4,9–13]. Culturing hiPSC-CM or human embryonic stem cell (hESC) derived cardiomyocytes (hESC-CM) within the *in vivo*-like micro-environment of Engineered Heart Muscle (EHM[14–23]), or MPS[24–28] has matured hiPSC-CM to some extent by enhancing physiologic hypertrophy, and led to pharmacology more closely correlated to the adult human heart. However, these approaches have not demonstrated consistent electrophysiological maturation of hiPSC-CM, and variability in baseline APD and beat rates make electrophysiology studies especially challenging[2].

In addition to 3D culture approaches, bioreactor-based strategies such as chronic electrical pacing or cyclic strain (typically applied over 2–4 weeks in culture) enhance maturity of hESC-CM and hiPSC-CM[17,20,29,30]. Collectively these methods are promising, but no single approach applied thus far has been sufficient to induce full maturation of pluripotent stem cell derived cardiomyocytes. Furthermore, many of the existing approaches require prolonged culture periods (in some cases approaching one month[29,31]), large scale formats, and/or complex setups to execute. These issues would lead to cost and logistical limitations for their translation to higher-throughput analyses that would be essential to use these technologies for drug development.

As bioreactor approaches have limited scalability, and tissue engineered microenvironments alone are not sufficient to induce hiPSC-CM maturation consistent with the adult heart, there has been a focus on combining tissue engineering approaches with soluble cues. Consistent with the notion that microenvironmental cues can enhance hiPSC-CM maturity, transplanting hiPSC-CM into neonatal rodent hearts enhances maturation[32]. One possible explanation for this result is that the milieu of the heart contains soluble cues that enhance cardiomyocyte maturity. Reductionist approaches have used specific soluble cues from the fetal and post-natal heart, including cytokines[33,34], micro-RNAs[5], heart specific extracellular matrix[35] and hormones[36] to enhance the maturity of hESC-CM and hiPSC-CM.

Metabolic cues like glucose levels provide another key facet of the heart's soluble environment that may be particularly important to cardiomyocyte maturation. Postnatally, the heart switches from glycolysis to fatty-acid oxidation as its primary source of ATP [37,38]. Previously, 2D hiPSC-CM monolayers and engineered tissues exposed to glucose-depleted, fatty-acid enriched media exhibited more mature metabolic profiles and physiology compared to hiPSC-CM cultured in standard media[7,31,39,40]. However, fatty-acid based media has not been studied in the context of MPS, and potential population variance in cellular response to fatty-acid media has not been explored.

We hypothesized that the combination of aligned 3D culture and fatty-acid could enhance electrophysiological maturation of hiPSC-CM within cardiac MPS. Previous studies have suggested high inter-patient variability in expression of metabolism-related genes in the heart, and that these differences are reflected in the transcriptome of patient-derived hiPSC-CM[41]. Thus, we tested the effects of MM in from two distinct donor lines labeled WTC[42] and SCVI20[43]. Both lines were derived from healthy individuals who did not harbor known cardiomyopathy-associated mutations. Using a Design of Experiments approach[44–46], in MPS derived from WTC hiPSC, we identified fatty-acid based Maturation Media (MM) that led to a more mature mitochondrial phenotype and improved calcium handling in MPS compared to standard media (SM). These changes were associated with shortened, adult-like Action Potential Duration (APD) in WTC-MPS. MM-treated MPS also exhibited changes in expression of ion-channel and calcium handling genes, including Sarcolipin (SLN). At baseline, monolayers and MPS derived from SCVI20 had extremely short action potentials. Whereas MM markedly shortened APD in WTC MPS, the same media prolonged APD in SCVI20 MPS. In both cases, MM treatment led to APD within the range of 300–450 ms expected for adult human left-ventricular cardiomyocytes[4]. In both genotypes, MM treatment led to a more mature mitochondrial structure and a stronger mitochondrial potential gradient, along with reductions in APD variability and a trend toward a more robust calcium transient ($\Delta F/F_0$) and enhanced contractility at low extracellular calcium. The ability to reduce APD variability and push the APD closer to the 300–450ms interval was confirmed in MPS made from two additional genotypes (SCVI273[47] and G15.AO[48]).

To understand these differential responses to common media, we used predictive computational models to determine the contribution of changes in specific currents, fluxes and calcium handling machinery to observed alterations in the action potentials and calcium transients. These models predicted that individual currents were different between immature MPS of different genotypes, despite both basal hiPSC having been derived from healthy male volunteers who did not harbor mutations strongly associated with disease. MM treatment led to a convergent set of adaptations to ion currents and calcium handling parameters, and the MM-induced changes in simulated currents were consistent with shifts in the pharmacology of MM versus SM. These results suggest that differences in the action potential and calcium handling of hiPSC-CMs from different lines may be exaggerated by the glycolytic milieu of standard cardiac media. Fatty acid-based maturation media can reduce these differences, while also reducing intra-sample variability from the same patient's cells, to allow more predictive drug testing.

Results

Screening for optimal carbon sourcing in hiPSC-cardiac MPS.

We first optimized fabrication of hiPSC-CM derived cardiac MPS[24] to enhance the consistency of multilayer tissue self-assembly (Fig. 1A–C) and subsequent achievement of aligned sarcomeres and uniaxial beating (Fig. 1D,E). To minimize batch-to-batch variability in cellular composition that might hinder drug screening studies, we formed cardiac MPS that mimicked the mass composition of the human heart by combining a defined cocktail[49] of 80% WTC hiPSC-CM and 20% isogenic hiPSC-SC (Supplemental Methods,

Supplementary Fig. S1 and Extended Data Fig. 1). We employed Robust Experimental Design to screen for the effects of glucose, oleic acid, palmitic acid, and albumin (bovine serum albumin, BSA) levels on WTC MPS maturity (Table S1). MPS were incubated with different fatty-acid media for ten days before their beating physiology and calcium flux were assessed. Optimal media would reduce automaticity (e.g. reduce spontaneous beating interval), while reducing the interval between peak contraction and peak relaxation (a surrogate for APD) in field-paced tissues (Extended Data Fig. 2A–C), and maintaining a high level of beating prevalence during pacing (defined as the percent of the tissue with substantial contractile motion; Extended Data Fig. 2D). Beating interval correlated with rate-corrected Full-Width Half Maximum calcium flux time, FWHM (Extended Data Fig. 2B,E), and beating prevalence correlated with calcium flux amplitude (Extended Data Fig. 2D,F). The strong correlations between calcium flux and contractile motion with respect to timing and amplitude suggest that none of the medias used in this screen disrupt calcium-contraction coupling.

Screening experiments did not suggest a significant role for either oleic or palmitic acid alone in inducing shortened beating intervals (Extended Data Fig. 2B), and trends toward increased calcium transient duration at intermediate levels of the fatty acids were not statistically significant (Extended Data Fig. 2E). However, these fatty acids did have effects on beating physiology in the context of concurrent glucose deprivation: completely omitting glucose while adding in galactose in MPS treated with media having only oleic acid or palmitic acid eliminated beating under 1Hz pacing. In contrast, treatment with glucose-free (galactose containing) media that was supplemented with both fatty acids (Media 9; Extended Data Fig. 2G) partially rescued this deficiency. This is consistent with the ability of hiPSC-CM to use both these fatty acids as ATP sources[40]. Thus, we concluded that the optimal media should include both palmitic and oleic acids. Furthermore, although absolute glucose deprivation would likely force fatty acid oxidation, and previous work has established galactose combined with fatty acids as a viable ATP source for healthy hiPSC-CM in monolayer cultures[40,50], we observed that in MPS, complete glucose deprivation dramatically reduced beating prevalence and calcium transient amplitude, even in the presence of 10mM galactose. This prompted us to adjust the glucose level media to a low but non-zero level of 0.5g/L (2.75mM; ~10% of the level in standard RPMI Media). This level is similar to the level glucose reported in recent studies that used fatty acids to induce iPSC-CM maturation[7,31].

As the inclusion of higher levels of BSA appeared to diminish beating interval without severely affecting prevalence or calcium flux, we concluded that an ideal maturation media would contain this higher level (2.5%, vs. 0.25% contained in standard B-27 supplemented media; Extended Data Fig. 2B,E). This led to a new Maturation Media (herein referred to as “MM”): glucose free RPMI basal media supplemented with 2% B-27, 0.5g/L glucose (2.8mM), 10mM galactose, 2.25% BSA (to a final concentration of 2.5% BSA, including the BSA contained in B-27), 125μM oleic acid and 100μM palmitic acid. MM exhibited a substantial portion of the beneficial effects of glucose free, fatty acid enriched media on reducing beating interval, without a concurrent loss of beating prevalence with 1 Hz pacing (Extended Data Fig. 2G, H).

Maturation-Media Induced Changes in Action Potential and Calcium Transients for WTC MPS.

In WTC MPS, MM reduced APD from the prolonged levels we observed for Standard Media (RPMI containing B-27 supplement; SM) treated MPS (Fig. 2A,B,E). Interestingly, however, switching from SM to MM had no measurable effects on APD or automaticity when hiPSC-CMs were cultured in confluent 2D monolayers (Fig. 2E, Extended Data Fig. 3A,B). GCaMP6f based analysis of Ca^{2+} handling revealed that baseline-normalized calcium amplitude ($\Delta F/F_0$) was significantly increased by fatty-acid based MM in WTC MPS (Fig. 2G). However, we did not observe a significant change in the maximum calcium upstroke velocity in paced tissues (Fig. 2H). Likewise, action potential upstroke timing was not significantly affected by MM pre-treatment, although there was a trend toward shorter action potential upstroke times in MM pre-treated WTC MPS and hiPSC-CM monolayers (Extended Data Fig. 3C).

Due to concerns about potential cytotoxicity of high levels of BSA and palmitic acid[51,52], we also repeated APD studies on WTC MPS treated with MM in which we independently varied levels of these two components. The complete absence of palmitic acid and reduction of BSA levels to those provided by B-27 alone from MM led to APD that was not significantly different from APD observed for SM treated MPS (M1; Extended Data Fig. 3G). In the absence of palmitic acid, the addition of a high dose of BSA appeared to be somewhat toxic to cardiac tissues, as the prevalence of beating in these samples (M2) was nearly zero, making it difficult to interpret the apparent APD (Extended Data Fig. 3H). Interestingly, palmitic-acid enriched media still had significant effects on APD reduction, while negative effects of high albumin dosing were slightly reduced, when the total amount of albumin present was reduced below 2.5%. However, since the APD observed with 1% BSA (M4; Extended Data Fig. 3G) was significantly lower than the APD for adult human left ventricular cardiomyocytes, we assumed these tissues might fall outside the ideal physiologic range for drug testing. Thus, MM with 125μM oleic acid, 100μM palmitic acid, 0.5g/l glucose, 10mM galactose and 2.5% BSA was used for all subsequent studies.

Although several types of fatty acids have been shown to enhance maturation of hiPSC-CM monolayers and engineered heart tissues, here we found that it was necessary to include palmitic acid specifically (Extended Data Fig. 3G). This suggests that although generalized metabolic effects such as oxidation-induced DNA damage response[7] are likely important to maturation of hiPSC-CM *in vitro*, events affected directly by palmitic acid, such as palmitoylation of calcium channel subunits[53] or receptors[54] may also be involved. Furthermore, although it was possible to reduce APD with maturation media that included oleic acid and palmitic acid without increased albumin (M4; Extended Data Fig. 3G), this treatment yielded APD that fell below the target range of adult cardiomyocytes. It is possible that albumin, which is a fatty-acid carrier *in vivo*, provided a more temporally stable dose of fatty acids to cells cultured within the MPS. The concentration of albumin in MM is not markedly dissimilar from the 3.5–5% albumin level found in human blood[55]. Finally, the finding that fatty-acid based maturation media had significant effects on action potential and pharmacology within WTC MPS, but not 2D hiPSC-CM monolayers, suggests the need

to incorporate advanced 3D co-culture models during development of protocols to mature hiPSC-CM, and likely other hiPSC-derived tissue cells.

Divergent effects of maturation media on action potentials in genetically distinct cardiac MPS.

Previous studies have suggested that hiPSC-CM provide an accurate representation of the transcriptome of isogenic human heart muscle, and intra-genotype variability among hiPSC clones from the same patient is minimal[41]. In contrast, the inter-patient variability in hiPSC-CM transcriptomes is significant, with metabolism-related genes being particularly variable across different patient genotypes. Thus, we hypothesized that fatty acid base maturation media would have differential effects in MPS formed from hiPSC-CM derived from different individuals. To address this hypothesis, we tested fatty-acid based MM in a genetically distinct set of hiPSC-CM, SCVI20. In contrast to WTC, SCVI20 exhibited much shorter APD at baseline, ranging from 250 to 350ms in monolayers and 150 to 400ms in MPS (Fig. 2C). Treatment of SCVI20 MPS for 10 days with MM prolonged APD, so APD_{80} fell within a similar range to what we observed for MM-treated WTC MPS (Fig. 2D,F), and within the range of 300 to 450msec observed for human adult ventricular cardiomyocytes[4,56]. Interestingly, analysis of Ca^{2+} handling using OGB-1-AM revealed that MM treatment produced a similar trend toward increased background normalized calcium transient amplitude ($\Delta F/F_0$) in SCVI20 MPS as it did in WTC (Fig. 2I). However, this trend was not statistically significant in SCVI20. Importantly, because GcaMP6f and OGB-1-AM have different affinity for Ca^{2+} and different quantum yield for Ca^{2+} induced fluorescence (K_D of 375nM for GcaMP[57] and K_D of 170nM for OGB-1[58]), one cannot directly compare the $\Delta F/F_0$ response between MPS derived from these different lines. Despite not enhancing $\Delta F/F_0$ in SCVI20, MM did significantly increase the maximum Ca^{2+} upstroke velocity in MPS of this genotype (Fig. 2J). There was no trend between media type and upstroke timing in SCVI20 MPS (Extended Data Fig. 3D).

The differences in $cAPD_{80}$ of SCVI20 and WTC MPS in response to MM prompted us to test the effects of this media on two additional iPSC lines, SCVI273 and G15.AO[48]. Compared to adult ventricular cardiomyocytes, MPS derived from SCVI273 hiPSC-CM initially had a prolonged APD, like WTC. Interestingly, MPS of the SCVI273 genotype responded similarly to WTC in terms of APD shortening effects of MM (Extended Data Fig. 3E and Extended Data Fig. 4A). However, there was no trend toward increased $\Delta F/F_0$ for Ca^{2+} (Extended Data 4F). In contrast to MPS made from SCVI273 iPSC-cardiomyocytes, G15.AO MPS behaved similarly to SCVI20 MPS: initial APD_{80} values were short and were prolonged by maturation media (Extended Data Fig. 4A). Despite these differences in prolongation versus reduction of $cAPD_{80}$, all MPS had two common outcomes when treated with maturation media. First, spontaneous beat rate was reduced by maturation media in all MPS from all four genotypes (Extended Data Fig. 4B). Second, variability in $cAPD_{80}$ and spontaneous beat rate was markedly reduced by treatment with MM, except for the case of spontaneous beat rate in G15.AO (Extended Data Fig. 4B).

Maturation Media Supports a Shift Toward a more Mature Mitochondrial Structure in hiPSC-Cardiac MPS.

Maturation-media induced changes in the state of mitochondria within iPSC-cardiomyocytes in MPS were next assessed. Mitochondrial inner transmembrane potential, as measured with MitoTracker Red, was markedly upregulated by MM in WTC (Fig. 3A–C), SCIV20 (Fig. 3D and Extended Data Fig. 5A,B) and G15.AO (Fig. 3E and Extended Data Fig. 5C,D), suggesting an increase in oxidative phosphorylation[59] in MM treated MPS. Antibody-staining revealed that overall mitochondrial density did not change, but mitochondrial organization shifted with MM treatment in all three genotypes (Fig. 3A,B and Extended Data Fig. 5A–D). SM produced short filaments and rounded structures, whereas MM treatment yielded a mitochondrial structure of extended filaments and networks. Similar filamentous networks of mitochondria, running perpendicular to Z-lines, have been observed previously during postnatal development of rodent cardiomyocytes[60]. Interestingly, although iPSC-cardiomyocyte monolayers treated with MM showed upregulation of maximum Oxygen Consumption Rate (OCR) in Seahorse assays, they did not show marked increased in mitochondrial membrane potential (Fig. 3C,D and Extended Data Fig. 5E,F,H–K). These data indicate that fatty acid-based MM directly alters the state of mitochondria in hiPSC-cardiomyocytes within the cardiac MPS, indicating a more mature metabolic phenotype in fatty-acid-treated iPSC-CM[7,40]. The finding that MM caused more substantial shifts in mitochondrial state in MPS as opposed to monolayer culture is consistent with our finding that MM caused less significant changes in physiology of monolayers as compared to MPS (Fig. 2). This may reflect a lower ATP consumption rate in monolayers, which are not doing active mechanical work, as contrasted to cardiomyocytes in MPS that contract against PDMS posts.

Pre-Treatment of hiPSC-Cardiac MPS with Maturation Media Supports Inotropic Responsiveness.

MM treatment did not result in changes in gross sarcomere structure within WTC or SCVI20 MPS, as assessed by staining for sarcomeric α-Actinin (ACTN2; Fig. 4A–B). Quantitative analysis of sarcomere morphology with Fourier-Transform based methods[50,61] was consistent with these qualitative observations, and suggested no substantial changes in sarcomere organization because of MM treatment (Extended Data Fig. 6A–B). Expression and localization of β-Myosin Heavy Chain and MLC-2v, two sarcomere-associated proteins which typically mark mature ventricular-like hiPSC-cardiomyocytes were similar in MM and SM pre-treated MPS (Extended Data Fig. 6C–G). There was a trend toward upregulation of MLC-2v protein in MM-treated SCVI20 MPS, consistent with previous observations that palmitic-acid enriched, glucose depleted media increased MLC-2v levels[7].

When we measured force developed in MPS via the deflection of PDMS pillars in the chamber (Supplemental Methods; Fig. S2), we found that both SM and MM-pre-treated WTC MPS exhibited a robust dose response to increased extracellular calcium, with a maximal range of stress similar to adult human heart tissue slices (Fig. 4C; data on adult slices ref.[56]). Consistent with prior work, we observed that fatty-acid based maturation media neither inhibited nor enhanced peak twitch force[7]. However, MM pre-treated WTC MPS were sensitized to lower concentrations of extracellular calcium than SM pre-treated

controls, with a statistically significant EC_{50} of 0.11±0.06 mM for MM pre-treated MPS versus 0.95±0.46mM for SM-pre-treated controls ($p < 0.05$, 2-way *t*-test). Furthermore, MM pre-treated MPS showed a statistically significant steeper fold-increase in force in response to extracellular calcium over the linear region of the calcium-force response curve, with an initial slope of 12±1.5 mN/mm^2/mM Ca^{2+} versus 3.9±0.26 for SM-pre-treated controls ($p < 0.01$, 2-way *t*-test). Consistent with the trend that MM-treatment enhanced Ca^{2+} handling ($\Delta F/F_0$) more significantly in WTC than in SCVI20 MPS, SCVI20 MPS also showed a trend toward increased force with MM, but even at low extracellular Ca^{2+} levels, the trend towards higher twitch forces with MM was not statistically significant (Fig. 4D).

Analysis of tissue inotropic responses to isoproterenol in MM pre-treated WTC MPS showed a trend toward desensitization, and MM-treated SCVI20 MPS showed a trend toward sensitization to this drug, though neither trend was statistically significant (Fig. 4E,F). Similarly to inotropic effects of isoproterenol assessed at constant (paced at 1Hz) beat-rate, MM pre-treatment appeared to slightly desensitize MPS to the chronotropic effects of isoproterenol in both genotypes, although, as with inotropic effects, the changes were not statistically significant (Fig. 4G,H). The EC_{50} values for isoproterenol chronotropy fell within the range recently reported for engineered heart tissue subjected to exercise-induced maturation via external pacing[29], and within the range of adult human heart slices[56].

Collectively, these data suggested that MM does not damage sarcomeres or interfere with excitation-contraction coupling or adrenergic responsiveness and enhances calcium contraction coupling when the amount of extracellular calcium is limiting. Furthermore, unlike the divergent trend observed with respect to MM-induced change in APD in SCVI20 vs. WTC, inotropic responsiveness showed a relatively similar trend in both genotypes, suggesting multimodal analysis of tissue function for accurate characterization.

Gene expression changes caused by maturation media in cardiac-MPS.

Consistent with previous studies, we observed genotype-based variability in transcription of monolayer hiPSC-CM in standard media[13]. However, there was no significant difference in a panel of ion channel and sarcomere related genes caused by MM treatment of monolayers of either genotype (Fig. 5A,B). Consistent with observations regarding the immaturity of hiPSC-CM, several ion channel transcripts were either deficient or overexpressed in these cells, when compared to commercially available RNA obtained from adult human hearts (Fig. 5A,B). Further, the absolute level of SCN5A (transcript for the Nav1.5 alpha subunit of I_{Na}) and several other ion channel transcripts, including KCNJ2 (transcript for the Kir2.1 alpha subunit of I_{K1}), was highly variable between different batches of purified, 2D monolayer hiPSC-CM. This may point to mis-regulation of expression in these channels in non-physiologic culture formats, or to differences in the relative levels of different cardiomyocyte sub-types obtained from our small molecule-based differentiation protocol[62,63].

We next assessed gene expression in MPS treated for ten days with either SM or MM. Interestingly, and in contrast to results by Mills *et al.*[7], we did not observe significant variation in expression of the glycolysis associated gene, GAPDH, relative to other potential “housekeeping” genes (data not shown). A lack of change in GAPDH expression on the

protein level was further verified by immunostaining, which revealed no significant effects of MM on GAPDH expression in either WTC or SCVI20 (Fig. S3).

Analysis of a panel of genes involved in electrophysiology, cell identity, contractility and calcium handling did not reveal a global shift in expression as would be expected for gross changes in cell differentiation or population composition in either genotype (Fig. 5C,D). Further, we did not observe substantial differences in the transcript expression for most potassium channels, including hERG/KCNH2 (related to I_{Kr}). However, MM-treated WTC MPS showed upregulation of SLN, HCN2 and CACNB2, and downregulation of KCND2 and ALDH1A1 (Fig. 5E). In SCVI20, MM treatment caused a trend toward decreased KCNJ2 (I_{K1}) and diminishing this current could be one explanation for increasing APD. We also observed KCND2 (I_{to}) upregulation. In contrast to I_{K1}, I_{to} contributes to early (rather than late) repolarization and would be expected to maintain the early repolarization trajectory without markedly altering APD_{80}. When treated with MM, SCVI20 MPS also showed upregulation of CACNB1 and SLN, although these changes were not statistically significant (Fig. 5F).

Sarcolipin (SLN) is known to bind the SERCA pump in the sarcoplasmic reticulum (SR) of cardiac and skeletal muscle, where it acts as a regulatory protein and is involved in thermogenesis[64]. It does so by partially uncoupling SERCA's calcium re-sequestration function from ATP hydrolysis and therefore burning extra ATP, without significantly influencing calcium homeostasis[65–67]. It is possible that since MM brings a higher caloric intake to the tissue through fatty acids, MM-treated MPS tissues might upregulate SLN to burn excess ATP. This would be consistent with more mature and efficient metabolism in MM through a metabolic switch from glycolysis to oxidative phosphorylation, which is supported by direct analysis of mitochondrial morphology and transmembrane gradients in MM-treated MPS (Fig. 3). SLN is preferentially expressed in atria and in previous work has been used to identify atrial-like hiPSC-cardiomyocytes[68]. However, the possibility that MM shifted cardiomyocytes in MPS toward atrial subtypes is contradicted by the overall pattern of gene expression – specifically, transcript levels for HEY2, a ventricular cardiomyocyte-specific transcription factor[69], were not affected by MM in WTC (Fig. 5C). Similarly, atrial cardiomyocyte specific transcription factor NR2F2[69] and sarcomere gene MYL7 were both downregulated by MM. Altogether, these data suggest that upregulation of SLN is more likely to be directly related to cardiomyocyte metabolism than tied to cardiomyocyte subtype.

The β-subunits of the voltage activated calcium channel expression encoded by CACNB1 and CACNB2 are required for expression of the *L*-type calcium current through regulating trafficking and activation of α-subunits[53,70]. Changes in expression of these subunits are noted altering I_{CaL} in heterologous systems and *in vivo*[71]. Despite our observation that force production and inotropic responsiveness of MPS were not perturbed by MM pre-treatment, we observed significant downregulation of several genes associated with calcium handling and sarcomere function in WTC, including MYL7, MYL2/MLC2V, and MYH7 (Fig. 5E,F). We observed a similar reduction of MYL2 and a trend towards decreased MYH7 in SCVI20. These consistent drops in expression for sarcomere-related transcripts are surprising given other studies that used chronic field pacing or fatty acid-based media to mature hiPSC-

cardiomyocyte tissues report an *increase* in these transcripts[7,29]. However, we also observed via immunostaining that levels and localization of the proteins encoded by the genes are not changed significantly, and trend toward upregulation with MM, in both genotypes (Extended Data Fig. 6). Further, despite relatively similar levels of MYL2 and MYH7 proteins in WTC and SCVI20, the contractile forces of WTC are substantially higher (Fig. 4C,D). Collectively, these data suggest that transcript level increases in expression of sarcomere genes may not be required for more mature physiology in hiPSC-derived engineered heart tissues.

Computational identification of ion currents and calcium handling mechanisms effects of maturation media.

Although MM has opposite effects on APD in SCVI20 vs. WTC MPS, in both cases, this fatty acid-based media brings tissues closer to an *in-vivo*-like ventricular APD, and matured Ca^{2+}-handling. Our transcriptomic analyses suggest that these convergent effects of MM result from an equally diverse range of adaptive mechanisms. This is to be expected given the different starting phenotypes. However, a key question, both for this study and hiPSC-CM platforms in general, is whether these convergent effects result from the underlying currents becoming similar between WTC and SCVI20 as a result of MM, or if they remain different even though the AP morphology and calcium handling converge. It is well known that many combinations of underlying currents can result in the same observable AP and Ca^{2+} transient[72,73]. Thus, if the underlying current ensemble remains different after maturation, the responses of the mature tissues to pharmacological or other perturbations will also be different. Unfortunately, because matured hiPSC-CMs cannot be viably extracted from the MPS, it was not possible for us to directly assess the currents underlying the immature and mature WTC and SCVI20 APs via patch-clamp electrophysiology. Instead, we have applied an established computational approach, which uses the simultaneous changes in AP morphology and intracellular Ca^{2+}, to determine the combination of currents most fit to elicit those changes (Fig. 6). The ability of this approach to identify changes to the major cardiac ion channels has been rigorously characterized in previous studies[28,74].This approach has been successfully applied to MPS data to distinguish multiplicitous molecular actions of major cardioactive drugs[27,75], to predict drug actions in short QT syndrome from patient-derived hiPSC-CM recordings[76], and to computationally mature the measured APD[28,74].

When applied to the WTC and SCVI20 recordings (Fig. 6), these analyses predicted enhancement of the rapid delayed rectifier potassium current I_{Kr} (hERG) in WTC (Fig. 6D), which would directly contribute to the observed APD shortening. No trends were observed for predicted I_{K1} in either genotype (Fig. 6E). In WTC MPS, simulations also predicted that MM reduced major inward currents, including I_{Na} and a major reduction in the sodium-calcium exchange current (I_{NaCaX}), with a further trend for reduced *L*-type Ca^{2+} current (I_{CaL}) (Fig. 6F–H). They also predict effects on intracellular calcium handling. In particular an increase in intracellular Ca^{2+} buffering in WTC (Fig. 6I, primarily a result of increased expression or Ca^{2+} affinity of the myofilaments), and trends toward improved intracellular calcium transport and RYR function with MM (Fig. 6J–K). In SCVI20 MPS, MM-treatment did not result in significant changes in any of the simulated currents or

calcium handling parameters described by the model. However, trends for subtle increases in the major inward currents (I_{Na}, I_{CaL}, I_{NaCx}) likely combine to explain the observed APD_{80} prolongation.

With respect to Ca^{2+} homeostasis, the simulations suggest that the increase in WTC calcium transient amplitude (Fig. 2G) is best explained by a shift in Ca^{2+} flux balance. Specifically, the major reduction (~75%) in I_{NaCaX} favors calcium influx over extrusion. This balance is the major determinant of whole-cell calcium load in cardiomyocytes[77]. Under conditions of increased whole-cell calcium, SR calcium would be expected to increase markedly, even without any changes in SERCA expression or regulation. To counteract some of this increase, the simulations predict diminished SERCA pump activity in the MM-treated WTC MPS (Fig. 6L). This is consistent with gene expression data predicting marked MM-induced upregulation of SLN in WTC MPS. SLN interacts with and suppresses SERCA pump function, such that even without alteration of SERCA expression, transport function is be reduced. In the case of MM-SCVI20, there was no significant change in $\Delta F/F_0$ compared to SM-SCVI20 (Fig. 2I). This is supported by the model showing a trend towards increases in both I_{CaL} and I_{NaCaX} (Fig. 6G,H). Since these two mechanisms counteract each other with respect to Ca^{2+} flux, but both generate dominant inward currents, they provide a combined mechanism that is consistent with both unchanged calcium transient amplitude ($\Delta F/F_0$) and prolonged APD_{80}.

We independently interrogated these effects on calcium handling through pharmacologic challenge via ryanodine mediated block of SR calcium release, and thapsigargin mediated block of SR calcium reuptake. Saturating ryanodine (10 mM) dramatically increased both Ca^{2+} rise-time and decay time (τ_{75}) in MM-pre-treated, but not SM pre-treated WTC MPS. Moreover, although Ryanodine diminished $\Delta F/F_0$ for both SM and MM pre-treated MPS, MM pre-treated MPS showed a more substantial change in $\Delta F/F_0$ in response to this drug (Fig. S4). Neither MM nor SM pre-treated MPS displayed a change in beat rate upon treatment with Ryanodine (Fig. S4A). Not only are these findings consistent with predictions from simulations of trend toward greater predicted steady state SR-storage of Ca^{2+} with MM (Fig. 6), they are also consistent with a trend toward greater RyR flux in MM treated WTC MPS (Fig. 6J). Thapsigargin also markedly slowed Ca^{2+} reuptake, increasing τ_{75}, in MM but not SM-pretreated MPS. In contrast to Ryanodine, Thapsigargin did not affect $\Delta F/F_0$ or calcium rise-time (Fig. S5). This response is consistent with our simulation data, which suggest that although SR calcium storage is enhanced by fatty acid media, there is some predicted suppression of SERCA activity (Fig. 6L). Altogether, these experimental results are consistent with the prediction of the simulations that pre-treatment with MM increases the SR Ca^{2+} store, and its contribution to the cytosolic Ca^{2+} transient that fuels contraction. These results are internally consistent with the results of our simulations, and with previous work in which matured hiPSC-CM exhibited a marked calcium decay time in response to thapsigargin[31]. In previous studies, maturation media containing dexamethasone and triiodothyronine[78], and maturation induced by continuous field pacing[29] have been linked to improvements in hiPSC-CM Ca^{2+} handling through formation of T-tubules. In the present study we observed minimal evidence of T-tubules, although qualitative analysis of Wheat-Germ Agglutinin stained MPS showed some instances of membrane invaginations that were more prominent in MM (Fig. 6A–C) than in SM (Fig. S6D,E) treated MPS.

In summary, these simulation-based analyses predict that the changes that normalize APD and calcium handling as a result of MM are different for WTC and SCVI20, but that as a result of those changes the mature phenotypes are very similar for the two lines. Indeed, changes to almost every ion current and calcium handling parameter described by the model (except for potassium currents and calcium buffering; Fig. 6D–E,J) were different for SCVI20 vs. WTC MPS. At the same time, MM-treatment led the final predicted currents and calcium handling to be nearly identical for SCVI20 and WTC. That is, no parameters predicted by the model differ between MM-treated SCVI20 and WTC MPS, except for I_{Kr} and calcium buffering, which were predicted to be higher in MM-treated WTC MPS (Fig. 6D,I). The observation that no single simulated current was significantly different in MM vs. SM treated SCVI20 MPS suggests the potential that SCVI20 hiPSC-CM emerge from cardiac differentiation in a more matured state than do WTC hiPSC-CM. However, this is debatable given the significantly higher force produced by WTC MPS in either SM or MM (Fig. 4C,D). Instead, a more parsimonious interpretation is that the changes in APD_{80} between SM and MM treated SCVI20 MPS (Fig. 2D,E,H) are caused by concurrent subtle changes in several of the currents that contribute to the action potential, whereas broader changes are required for WTC.

Maturation media affects pharmacology of cardiac-MPS.

We next assessed whether MM treatment could lead to more predictive pharmacology of compounds with known effects on action potential morphology and contractility, and whether the simulation framework applied to the mechanisms of maturation could more readily identify those drug actions in MM-pre-treated MPS. Pro-arrhythmic outcomes of these drugs have been quantified in clinical studies by measuring QT interval[79], among other determinants of arrhythmic potential. An important drug from these studies is Verapamil, which blocks both I_{CaL} and I_{Kr}, and is routinely used in the clinic to shorten the QT interval in patients prone to suffer arrhythmias based on prolonged APD (for example, patients with long-QT syndrome[79]) based on I_{CaL} block. Verapamil is a prototypical example of a “false positive” drug that would appear to prolong APD and QT interval if one only applied standard assessment of block of the current encoded by hERG/KCNH2, I_{Kr}[79,80].

When we analyzed Verapamil dose-escalation effects in field-paced MPS and used beating prevalence as the metric for characterizing IC_{50}, we observed that MM-pre-treated WTC MPS exhibited enhanced Verapamil resistance compared to SM-treated MPS (971 nM for MM-pre-treated MPS, versus 90nM for SM-treated MPS; Fig. 7A). In contrast, SCVI20 MPS showed a decreased Verapamil resistance with the same media (Fig. 8A). Direct analysis of APD revealed a dose-dependent decrease in APD_{80}, consistent with the clinical application of this drug to shorten QT duration (Extended Data Fig. 7A,B). However, unlike beating prevalence, the dose-response for APD_{80} did not change appreciably in MM pre-treated, compared to SM-pre-treated MPS, for either genotype. There were, however, weak trends toward Verapamil desensitization in MM-treated WTC and Verapamil sensitization in MM-treated SCVI20 MPS when APD_{80} was used as an *in vitro* metric of drug response (Fig 7B, 8B).

These genotype-based shifts in Verapamil responsiveness may be explained by the relative I_{CaL} and I_{NaCax} levels predicted by mathematical models (Fig. 6G,H): in WTC, the trend with MM is toward slightly higher I_{CaL} (increases intracellular Ca^{2+}) and markedly lower I_{NaCax} (decreases intracellular Ca^{2+}). The net effect of this increases influx and diminished efflux would be higher steady state levels of Ca^{2+} stored in the SR. Higher SR-calcium levels would tend to increase contractility in response to Ca^{2+} uptake through *L*-type calcium channels, thereby desensitizing cells to I_{CaL} block. Increased steady state Ca^{2+} levels would also be consistent with the observed increase in calcium amplitude ($\Delta F/F_0$; Fig. 2G) and contractility in MM-WTC relative to SM-WTC MPS, in the setting of limiting extracellular calcium (Fig. 4C). In contrast, within SCVI20 MPS, the trend toward a stronger increase in I_{NaCax} than in I_{CaL} would result in lower SR levels of stored Ca^{2+}. This would likely make cells more sensitive to I_{CaL} block.

We next assessed the ability to predict pharmacology of Flecainide, a class Ic (Na^+ channel blocker) antiarrhythmic drug typically used to treat tachy-arrythmia, has been noted to have a narrow therapeutic index and is contra-indicated in patients with pre-existing structural disease[81]. This drug also blocks the hERG current[82]. Consistent with this narrow therapeutic index, we correctly observed very little difference between the Estimated Therapeutic Plasma Concentration (ETPC) of 1.5μM, and *in vitro* EC_{50} (APD_{80}) and IC_{50} (beating prevalence) (Fig. 7C,D, Fig. 8C,D and Extended Data Fig. 7C,D). Unlike Verapamil, Flecainide did not exhibit a differential EC_{50} within MM versus standard media pre-treated MPS for the WTC genotype; however, there was a weak trend toward desensitization of MM-pre-treated WTC MPS to the APD prolonging effects of this drug, which is consistent with improved hERG current in MM-treated WTC MPS. In the SCVI20 genotype, we observed a marked desensitization of MM-treated MPS to both contractile and APD changes induced by Flecainide. Although MM increases APD in SCVI20 MPS, the fatty acid media still causes a trend (albeit, not statistically significant) toward increased hERG current (Fig. 6D). Improved hERG current would desensitize MM-treated SCVI20 MPS toward I_{Kr} blocking effects of Flecainide.

Given how sensitive the SM-treated SCVI20 MPS are to the AP altering effects of Flecainide (EC_{50} of 5.5nM), the depressed contractility at 1 Hz pacing may be due to impaired calcium uptake. To test this hypothesis, we compared Ca^{2+} amplitude using OGB-1-AM imaging. This analysis revealed that, concurrent with lengthening the calcium transient timing, Ca^{2+} amplitude increased almost 3-fold over baseline in MM-SCVI20 MPS treated with 1μM Flecainide. In contrast, the amplitude of Ca^{2+} did not exceed baseline in Flecainide treated SM-SCVI20-MPS (Fig. S7A–C). The sodium-calcium exchanger can operate in reverse during action potential prolongation[83]. Thus, the observed ability of MM-SCVI20 MPS to withstand the contractility-depressing effects of Flecainide at doses that significantly disrupt contractility in SM-SCVI20-MPS may potentially be explained by the trend in simulations (Fig. 6H) toward enhanced I_{NaCax} in MM vs. SM pre-treated SCVI20 MPS. The observation that although Ca^{2+} uptake increases near 1μM Flecainide, but that contractility (beating prevalence) did not increase at this dose in MM-SCVI20 MPS, may potentially be explained by Flecainide-induced RYR block[84,85]. Consistent with the exaggerated effects of flecainide on APD in SM-treated SCVI20 MPS, MPS of this

genotype were more prone to Delayed After Depolarizations (DADs) than MM-treated MPS at 100nM dose of this drug (Fig. S7D,E).

Finally, we assessed MPS pharmacology of Alfuzosin, an α_1-adrenergic blocking agent that has been shown to increase patients' QT interval by hERG-independent mechanisms[13,86]. This causes Alfuzosin to appear as a "false negative" drug in screens for potential QT prolongation that rely on overexpression of the hERG/KCNH2 gene in heterologous cell types. Here, we observed that in WTC, both MM and SM pretreated MPS exhibited IC_{50} near 1μM when measuring beating prevalence (Fig. 7E). However, when we tested the effects of this drug on extending APD_{80}, we observed a specific sensitization with MM-pre-treated MPS, relative to MPS pre-treated with SM (Fig. 7F). We can explain the drastic change in APD with an unchanged prevalence through the efficient calcium transport of the MM-WTC, enabling the cells to contract despite the short resting time between long-duration actional potentials. In SCVI20, there was a trend toward sensitization of SM-treated MPS to Alfuzosin, although differences in the EC_{50} observed via APD_{80} analyses were not statistically significant (Fig. 8F).

We summarized these observations of drug responsiveness by plotting the safety margin observed for each drug, using either beating prevalence (Fig. 7G, 8G) to obtain IC_{50} or APD_{80} prolongation (Fig. 7H, 8H) as the metric used to obtain EC_{50}. The safety margin is defined as *in vitro* IC_{50}/ETPC for prevalence and APD_{80} for Verapamil (or *in vitro* EC_{50}/ETPC for APD_{80}), and describes the relative risk for beating abnormalities. Typically during pharmaceutical development, a safety margin of 18–20 (green line on Fig. 7G,H and 8 G,H) is used as a go/no-go decision for a chemical compound. None of these drugs exhibited differential pharmacology between SM and MM-pre-treated 2D monolayers in either genotype (data not shown). Safety margin analysis revealed that for WTC, culture within MPS and the subsequent maturation of MPS with fatty-acid enriched media had improved the safety margin for Verapamil (using the metric of prevalence) and Alfuzosin (using the metric of APD_{80}), but no statistically significant effect on the safety margin of Flecainide (Fig. 7G). There was also a trend, albeit not statistically significant, toward improved safety margin of beating prevalence to Alfuzosin in MM pre-treated MPS, compared to 2D monolayers. In SCVI20, MM-treated MPS showed improved prevalence safety margins (closer to target green line) in the three drugs when compared to 2D platforms (Fig. 8g). APD_{80} based safety margin gave improved results for both SM and MM-treated MPS for Alfuzosin and Verapamil (although not significant for the latter one) (Fig. 8H). SCVI20 MM and SM treated MPS tissues were hypersensitive to Flecainide when looking at the APD_{80} safety margin, to the point that *in vitro* EC_{50} was less than the clinically reported ETPC (Fig. 8H).

Besides being self-consistent with predictions of relative levels of specific currents (e.g. I_{Kr}, I_{CaL}) in MM vs. SM treated MPS of each genotype, these pharmacology data suggest that MPS improves the prognostic capability of hiPSC-CM, and that MM pre-treatment further augments the prognostic power of MPS. For example, although Verapamil is routinely used in the clinic, particularly for QT-interval management, it exhibits false positive toxicity in hERG-assays, and the beating prevalence of 2D monolayer cultures of hiPSC-CM are sensitized to this drug, as shown here (Fig. 7G and 8G) and in other studies[13,15,24]. Our

data suggests that culture within MPS alone dramatically enhances the IC_{50} of this drug, eliminating the false positive toxicity seen in 2D monolayer hiPSC-CM, regardless of genotype. These observations are consistent with our previous studies[15,24]. The combination of MPS with MM gives a more accurate profile of the safe nature (thereby reducing false positive toxicity) of this drug. In contrast, the fact that Alfuzosin is sometimes observed to cause arrhythmias in the clinic[86], suggests that the higher *in vitro* EC_{50} values observed in monolayer culture and SM-cultured MPS under-predict potential toxicity (false negative). Our findings with MM-cultured MPS, which indicate sensitization to the APD prolongation effects of Alfuzosin, suggest that MM pre-treatment enhances the ability of MPS to accurately predict the clinically observed effects of this drug.

Collectively, these data indicate that combining MPS culture with MM can reduce both false positive (Verapamil) and false negative (Alfuzosin) drug response estimates. Enhanced drug resistance is not universally observed in MPS culture, suggesting against the trivial explanation that drug availability is limiting in these 3D systems, likely due to the small and physiologically-relevant scale of our 3D microtissues ~ 150μm in width, consistent with cardiac muscle bounded by collagen fibrils[87]. Our work suggests instead that changes in drug susceptibility are due to changes in density and function of specific ion channels that these drugs target.

Conclusions

We demonstrated that the combination of aligned 3D culture in MPS with fatty-acid based media synergized to promote maturation of hiPSC-CM action potential. Variability in action potential waveform and calcium handling initially observed in standard glucose-based cardiomyocyte media were minimized by treatment with fatty acid-based media and converged within a range that is typical for adult human ventricular cardiomyocytes. Intra-sample variability in APD and spontaneous beat rate in MPS derived from multiple differentiation batches of the same hiPSC genotype were also substantially reduced by maturation media. Combining *in silico* modeling with experimental measurements provided insights into a putative mechanism linking fatty acid media exposure to alterations in individual ion channels and calcium handling machinery to whole-cell changes in action potential. This is the first study to induce maturation of hiPSC-CM in a microfabricated tissue-chip, and importantly, we demonstrated that maturation not only affected the baseline physiology of hiPSC-CM, but also yielded cells with pharmacology more reminiscent of adult human cardiomyocytes. Collectively, these results suggest that maturation with fatty-acid based media may be a prerequisite for drug discovery and safety testing with hiPSC-derived heart muscle.

Experimental Procedures

Cell Sourcing.

Two parent hiPSC were used in the majority of these studies: Wild Type C (WTC) human hiPSC harboring a single-copy of CAG-driven GCaMP6f knocked into the first Exon of the AAVS1 “safe harbor” locus[42] . The parent cell line (WTC) was reprogrammed from fibroblasts derived from a healthy 30-year-old Japanese male with a normal

electrocardiogram and no known family history of heart disease and is available from the Coriell Repository (# GM25256 hiPSC from Fibroblast). The second line, Stanford University Cardiovascular Biobank Line 20 (SCVI20), was generated from a healthy, disease genotype-free 77-year-old Caucasian male[43]. The third cell line, SCVI273, was generated from a healthy 43-year-old Asian female[47], and was used for comparison of action potential duration and calcium F/F_0 in response to maturation media treatment. SCVI20 and SCVI273 are available from the Stanford University Cardiovascular BioBank. The fourth cell line, G15.AO[48], was generated from mesenchymal stem cells derived from adipose tissue (ADSCs) using retroviral vectors coding for the reprogramming factors SOX2, OCT4, cMYC, and KLF4. It was used for comparison of action potential duration and to determine the metabolic profile in response to maturation media treatment. G15.AO is available from the Barcelona Stem Cell Bank.

Cardiomyocyte Differentiation.

hiPSC-CM were derived from pluripotent hiPSC and purified using published protocols relying on small molecular manipulation of Wnt signaling[88], with some modifications. Briefly, frozen stocks of pluripotent cells were thawed and plated on hESC-Qualified Matrix (Corning; Corning, NY) in Essential 8 Medium (E8; Thermo Fisher, Tewksbury, MA) containing 10μM Y27632 (Peprotech; Rocky Hill, NJ). Fresh E8 without drug was added the following day. To prepare cells for differentiation, hiPSC were grown to 70–80% confluency, and then passaged three times at a constant density of 20,000 cells/cm^2 (Burridge *et al.* 2014). During passaging, cells were singularized with Accutase (Thermo; Waltham, MA) and plated in E8 with 10μM Y27632. After pre-passaging, hiPSC were plated at a density of 25,000 cells/cm^2, in 10μM Y27632. This was counted as “day – 3” of differentiation. At day 0, hiPSC were >90% confluent and were treated with Roswell Park Memorial Institute Medium 1640 (RPMI) containing B-27 supplement without insulin (RPMI-I), along with 8μM CHIR99021 (Peprotech) and 150μg/mL *L*-ascorbic acid (LAA). Exactly 24 hr after drug was added, medium was exchanged for RPMI-I (day 1). On day 2, medium was replaced with RPMI-I containing 5μM IWP-2 (Peprotech). On day 4, medium was exchanged for RPMI-I. RPMI containing standard B-27 supplement (RPMI-C) was added on days 6,7,9, and 11. Robust spontaneous contractile activity was typically observed on day 8 of differentiation.

On day 15 of differentiation, hiPSC-CM were singularized and cryopreserved. Briefly, cells were washed twice, for 15 minutes, with dPBS, to deplete calcium from extracellular space and sarcomeres. Next, cells were exposed to 0.25% Trypsin (Thermo Fisher) for 10–20 minutes. Cells were triturated gently at every five minutes, then pelleted (300g, 5 minutes). Cell pellets were resuspended into RPMI-C with 10μM Y27632 for counting. Cells were then pelleted a second time, and resuspended into cryopreservation medium containing 10μM Y27632, then frozen and kept in liquid nitrogen.

Two weeks before MPS experiments, hiPSC-CM were thawed and plated at a density of 100,000 cells/cm^2 onto Matrigel, in RPMI-C with 10μM Y27632. The following day, medium was exchanged for RPMI-C. Three days after plating, monolayers were spontaneously contracting. Cells were then washed with dPBS and exposed to a

cardiomyocyte selective medium depleted of glucose and pyruvate (Media-L; RPMI 1640 without glucose or sodium pyruvate, supplemented with 23mM sodium bicarbonate and 5mM Sodium *L*-lacate[89]) for a total of five days. Cells were washed with dPBS and fresh Media-L was added every other day. On the fifth day of purification, significant death of non-beating cells was observed. Cells were washed with dPBS and allowed to recover in RPMI-C for three days. Cardiomyocyte purity both before and after this procedure was characterized by flow cytometry for Cardiac Troponin T (TNNT2; Table S2; Fig. S1).

Isogenic Stromal Cell Differentiation.

Isogenic iPS-stromal cells (hiPSC-SC) were derived via small molecular activation of Wnt signaling in pluripotent hiPSC, followed by VEGF exposure, as described previously[90]. Briefly, hiPSC were seeded at a density of 25,000 cells/cm^2 onto hESC-Qualified Matrigel. This was termed “day −3” of the culture. On day 0, wells were 80–100% confluent, and the medium was switched to LaSR media (Advanced F12/DMEM, 2.5mM Glutamax; 60ug/ml ascorbic acid), and 7.5uM CHIR99021 for 2 days without medium change. At day 2, the media was changed to LSR media with 50 ng/ml VEGF (Peprotech) for 2 days without medium change. On day 4, medium was replaced to LaSR media only. On day 6, cells were ready for CD31 magnetic sorting. For magnetic sorting on day 6 of differentiation, cells were rinsed with dPBS and trypsinized for 8min. Trypsin was quenched by adding EB20 media (20% FBS, 2.5mM Glutamax, KO DMEM), and cells were centrifuged (300g for 3 minutes) and re-suspended in FACS buffer (PBS, 2% FBS). CD31+ magnetic Dynabeads were added to the cell suspension at a concentration of 8 beads per CD31+ cell and left 20min on ice. The CD31 negative fraction was then expanded (maximum of ten passages) on uncoated tissue culture plastic substrates supplemented with EGM-2 media (Lonza) and characterized (Fig. S3). Full details on antibodies are provided in Table S2.

Plating of hiPSC-CM for 2D Monolayer Studies.

In 2D monolayers, hiPS-SC overgrow hiPSC-CM (data not shown). Thus, for 2D pharmacology and gene expression studies, biochemically purified hiPSC-CM were grown in monolayers. Purified cardiomyocytes were singularized with 0.25% trypsin after extensive dPBS washes. The cells were then resuspended into RPMI-C supplemented with 10μM Y27632 and plated at a density of 200,000 cells/cm^2 onto GFR Matrigel. The following day, medium was exchanged for RPMI-C. Three days after plating, monolayers were spontaneously contracting. Cells were then exposed to either SM or MM for ten days prior to the onset of gene expression and pharmacology studies.

Fabrication of Cardiac MPS.

Microfluidic cardiac MPS systems were formed using small modifications of the protocol described in our previous work[24] (see Fig. 1, Fig. S2). Briefly, two-step photolithography was used to form a chip comprised of: 1) a cell-loading port leading to a cell culture chamber with two large “anchoring posts” and several smaller micro-posts; and, 2) a media-loading port leading to media channels running alongside the cell culture chamber. The media channels and cell culture chamber (50μm high) are connected by a series of fenestrations (2μm x 2μm high/width) that provide a barrier to convective flow at defined volumetric flowrates, such that all media factors delivered to cells in the culture chamber

arrive via diffusion[24]. The cardiac MPS is formed by replica molding Polydimethylsiloxane (PDMS; Sylgard 184 kit, Dow Chemical, Midland, MI) at a 10:1 ratio of Sylgard base to crosslinker from a photolithographically defined wafer. These PDMS chambers were then bonded to glass slides using oxygen plasma.

Self-Assembly of Cardiac Microtissues within Cardiac MPS.

hiPSC-CM and hiPSC-SC (passage 5 – 8) were singularized with 0.25% trypsin after extensive PBS washes. We then prepared a cocktail of 80% hiPSC-CM and 20% hiPSC-SC, at a density of 6.6×10^6 cells/mL, in EB20 media supplemented with 10μM Y27632 and 150μg/mL *L*-ascorbic acid. 3μL of this cocktail, corresponding to 2×10^4 cells, was injected into the cell loading inlet of each MPS. MPS were then loaded by centrifugation (300g, 3 minutes), and plugged with an SP20 steel rod to prevent cellular regurgitation from the cell chamber during media loading. Next, the same media used to resuspend cells was added to the channels of each MPS. MPS were then individually inspected, and any cell chambers that were not completely filled were filled by applying gentle pressure to the SP20 plug. This time-point was counted as MPS day 0. At MPS day 1, media was changed to RPMI with B27 supplement. At day 3 MPS were continuously fed either maturation media or standard media, using negative pressure for media exchange as described in our previous study[24]. Pump-free, gravity-driven flow was used to feed the tissues. Every 2 days, fresh media was replenished into the inlet reservoir so that hydrostatic pressure would drive a continuous flow through the media channels to the outlet reservoir. This technique is commonly used with microfluidic devices due to its simplicity and low cost[91]. Potential batch-to-batch variability in hiPSC-CM phenotype was mitigated by performing all physiology and gene expression studies with MPS and monolayers derived from a minimum of three independent differentiations.

Robust Design Experiments to identify the composition of the optimal maturation media.

We hypothesized that switching the carbon source of cardiac MPS from glucose to fatty acids could induce more mature action potential waveforms and calcium transients in hiPSC-CM. We employed Robust Design screening to optimize four different media composition variables. Given the likelihood of these variables acting in a synergistic fashion to enhance maturation, the parametric space would require 3^4, or 81 independent experiments (excluding the several replicates required for significant studies). To study this large space in a cost and time-effective manner within MPS, we employed Robust Design[46] screening. With orthogonal arrays, the variable-space spanned by these 81 independent experimental conditions was explored with only 9 independent experiments. These 9 experiments were designed such that the four media input variables (levels of glucose, oleic acid, palmitic acid and BSA) were varied in an orthonormal fashion from one experiment to the next (Table S1). BSA (Sigma # A2153) was used directly, without being first stripped of exogenous fatty acids.

In the case where glucose was completely omitted from cardiac media, we added 10mM galactose, as previous studies have shown healthy hiPSC-CM are capable of using galactose as an ATP source[40,50]. Based on the hydrophobic nature of the primary fatty acids used as ATP sources in the heart (oleic acid and palmitic acid, respectively), we added additional

BSA, above the 0.25% already contained in the B27 supplement. In all cases where fatty acids were added to media, they were first incubated at 37°C with concentrated BSA and B27 supplement to allow fatty acids to bind the extra albumin, or the 0.25% albumin already contained in B27. Beating physiology and calcium flux were assessed with high-speed microscopy as described below. Media were screened based on their ability to reduce spontaneous beat-rate, as well as the interval between peak contraction and peak relaxation during 1Hz field pacing, while maintaining a high prevalence of beating (defined as the percent of the tissue with time-averaged motion exceeding a pre-determined threshold) during pacing at 1Hz. MPS were treated with various candidate maturation media for 10 days before beating physiology was assessed.

Image Acquisition for Beating Physiology Studies.

During imaging, MPS or 2D monolayers in multi-well plates were maintained at 37°C on a stage equipped with a heating unit (Tokai Hit, Gendoji-cho, Japan). First, baseline readings of spontaneous calcium flux (GCaMP6f), and beating physiology (bright-field video) were taken. After acquiring spontaneous electrical activity, electromechanical activity under field pacing was assessed. MPS were paced via sterile, blunted stainless steel needles that were inserted into the pipette tips leading to both the media inlets and outlets. Care was taken to fill pipettes and prevent bubble formation to maintain electrical conductivity. Before recording videos, cells were paced for 10 seconds (20V, 20msec bipolar pulses at 1Hz, ION OPTIX Myopacer Field Simulator). Pacing was then maintained at the same intensity and frequency for acquiring images of MPS contracting at 1Hz.

Imaging was performed with a NIKON TE300HEM microscope equipped with a HAMAMATSU digital CMOS camera C11440 / ORCA-Flash 4.0. All videos were recorded at a framerate of 100 frames/second for a duration of 8 seconds. For GCaMP imaging, fluorescent excitation was provided by a Lumencor SpectraX Light Engine (GCaMP: Cyan LED, 470nm) and filtered with a QUAD filter (Semrock). Videos were acquired using Nikon NIS Elements software.

Image Analysis.

Brightfield videos were analyzed for beating physiology using an updated version of our open source motion tracking software[42] (software available at https://huebschlab.wustl.edu/resources/). The current version of the software uses tools from the open source Bioformats Toolbox[92] to obtain image and metadata from microscopy files.

Briefly, microscopy files (Zeiss Zen; .czi) were directly read into the Matlab-based GUI, and the contractile motion of tissues was analyzed via an exhaustive-search block-matching optical flow algorithm that compared the position of 8×8 pixel macroblocks at frame i to their position at frame i+5 (corresponding to the motion in 50msec). Motion vectors were used to calculate beat-rate, beating interval (defined as the time delay between maximum contraction velocity and maximum relaxation velocity, which is directly proportional to action potential duration), and beating prevalence. Beating prevalence was defined as the percentage of macroblocks within a region-of-interest (ROI) with a time-averaged contraction speed that exceeds a defined threshold (2μm/sec was defined empirically as

a universal threshold for all MPS analyzed). ROI were selected to include the entire cell culture chamber of the MPS.

GCaMP data were quantified using in-house Matlab code that was developed based on previous work by Laughner and colleagues[61,93]. GCaMP videos were analyzed for τ_{75} decay time (time for calcium amplitude to go from maximum to 25% of maximum), Full Width Half Maximum (FWHM, time for calcium amplitude to go from 50% of maximum during upstroke, to 50% of maximum during decay) as well as peak intensity, a metric of total calcium influx. For spontaneously beating cells, data on beating interval and calcium transient decay times were rate corrected using Fridericia's method[94].

Optical Measurement of Action Potentials.

BeRST-1 dye was synthesized, and purity verified, as previously described[95]. For action potential recording, MPS were first labeled overnight with 2.5μM BeRST-1. The following day, MPS were equilibrated to media without dye before imaging (RPMI-C without phenol red) as described above, using a Red LED (640nm). For monolayer experiments, cells were labeled with 500nM BeRST-1 for 1h at 37°C, and then equilibrated to RPMI-C without phenol red. After acquiring videos of spontaneous and 1Hz paced activity at 100 Hz for 8 seconds, BeRST-1 videos were analyzed using similar Matlab code as was used for GCaMP analysis[93]. BeRST-1 videos were analyzed for 80% Action Potential Duration (APD_{80}). Reported values of APD_{80} (Fig. 2) are for MPS or monolayers paced at 1Hz.

MPS Tissue Isolation and Immunofluorescence Imaging.

Tissues were treated with SM or MM for 10 days. On day 10, MPS were flushed for 10 minutes with PBS at 25°C. Following this wash, 4% PFA was added to the media channel for 15min to fix the tissues. MPS were washed with PBS twice for 5min after that and were then carefully cut with a clean scalpel, to open the device and expose the tissue. At this point, the PDMS component had the tissue structure attached to it. The tissues were then stained by submerging PDMS blocks in different staining solutions: First, tissues were blocked with blocking buffer (1% BSA 10% FBS 0.5% Triton 0.05% sodium azide) overnight at 4°C. The next day, they were submerged the primary antibodies (Mouse anti α-actinin, Life technologies 41811; Rabbit anti-GAPDH, abcam 9485; Mouse anti-mitochondria, abcam 92824; Mouse anti β-myosin heavy chain, abcam 97715; Rabbit anti myosin Light Chain 2V (MLC2V), Proteintech 10906-1-AP) 1:100 concentration in blocking buffer) for 48h at 4°C. Tissues were then washed twice at 25°C in blocking buffer for 2–3 hours and washed a third time at 4°C overnight. The secondary antibodies (Goat anti-mouse IgG Alexa 568 H+L, Life Technology a11004; Goat anti-rabbit IgG Alexa 488 H+L, Life Technology a11008) along with 1:600 DRAQ5 (Abcam, ab108410) was incubated in blocking buffer for 24h. Tissues were then washed twice at 25°C in blocking buffer for 2–3 hours and a third time at 4°C overnight before tissues were imaged.

Both WTC and SCVI20 tissues were imaged with Opera Phenix™ High Content Screening System. All images were taken through proprietary Synchrony™ Optics 63x water immersion lens. Images were acquired using Harmony software. We imaged both DRAQ5 and α-actinin for sarcomere alignment using 640nm and 546nm lasers respectively. We

performed z-stacks over 60μm with a step-size of 0.5μm for α-actinin or GAPDH stains. Mitotracker and anti-mitochondrial antibody were imaged with a step size of 0.3μm. Post imaging processing was performed on ImageJ to enhance contrast and decrease background fluorescence. The same post-processing was performed for SM and MM tissues to allow direct comparison between them.

To analyse the regularity of sarcomeres from staining of sarcomeric α-Actinin, we applied Fast Fourier-Transform (FFT) based methods[61] to cellular regions of the MPS that had a constant size (100 × 100 pixels). Next, the real component of the FFT was smoothed with a 3×3 Gaussian filter, and the mean intensity was calculated as a function of radial distance from the centre of the centred real component of the FFT. Structures with regularly repeating features (e.g. sarcomeres) produce distinct bands when analysed in this manner, resulting in local increases in intensity at specific radial distance. These local intensity increases were quantified[50,61]. Code is available from the authors upon request. Representative fields of interest for intensity quantification and analysis of sarcomere regularity (Extended Data Fig. 6) were selected and analysed by a user blinded to the experimental condition.

Analysis of Mitochondrial Morphology and Potential.

Mitochondrial potential was analysed in 2D monolayers and MPS using MitoTracker Red (M7512 Thermo Scientific). Live MPS and monolayer were incubated with Mitotracker for 30min at 37°C in RPMI 1640 supplement with insulin. Samples were then washed with PBS for 10min before being fixed in 4% PFA for 15min and washed again with PBS. Monolayers were directly imaged, while tissues were isolated from the MPS as described above and placed into wells of 24-well plates with PBS until they were imaged.

Measurement of contraction force.

Micro-molded PDMS pillars were added to the cell chambers, so that the tissue would deflect them upon each contraction (Fig. 1B, S2A,B). By considering each pillar as a cantilever beam fixed at one end and uniformly loaded with horizontal forces along its height, one can apply the Euler-Bernouilli formula for uniformly distributed load and deduce the contraction force from the pillar's elastic modulus, deflection and dimensions. For WTC-MPS, pillar deflection was calculated with ImageJ by measuring the distance between the pillar's centroid coordinates before and after contraction. Same scale (0.5 pixel/micron) was used for all measurements.

To facilitate higher-throughput measurements, a new python-based software was developed to automatically identify pillars in the tissue. The software combined information derived from circle Hough transform[96] and custom template matching[97] algorithms (Fig. S2C) to detect the initial coordinates of the pillars at frame 0 of each recording. These initial positions were then fed to an enhanced version of our original tracking algorithm[42] to retrieve the absolute motion of the pillars during contractions (Fig. S2D). The motion was then converted to contraction force by using Euler's beam theory as described previously. This higher throughput software was used for SCVI20 MPS force analysis.

Pharmacology in MPS and 2D Monolayers.

To avoid any possible confounding effects that different albumin or lipid content might have on drug bioavailability[98], for all pharmacology, MPS were first equilibrated to phenol red free RPMI with B-27 (SM) containing vehicle control (DMSO, methanol, or water, to a final concentration of 0.1% v/v). On the day upon which studies were performed, freshly measured drug was dissolved into DMSO, except for Flecainide, which came as a methanol stock solution, and Verapamil or Isoproterenol, which were dissolved directly into media. For testing inotropic responsiveness to extracellular calcium concentration, Tyrode's saline (0.1g/L anhydrous $MgCl_2$, 0.2g/L KCl, 8g/L NaCl, 50mg/L anhydrous monobasic sodium phosphase, 1g/L D-glucose) was used in lieu of RPMI-C, as in previous studies of inotropic responsiveness of macroscale and miniaturized EHM[15,19]. After recording activity in zero-dose vehicle condition, media were exchanged for the lowest drug dose, and MPS were incubated for 30 minutes at 37°C. Spontaneous activity, and activity with 1 Hz pacing, were recorded as described above. This was repeated for each dose escalation of drug. Drug dose was escalated until all spontaneous and paced activity ceased, or a dose of 10μM was reached.

Media on monolayers of hiPSC-CM was replaced with phenol red free RPMI-C containing 1μM BeRST-1, and monolayers were incubated for 30 minutes at 37°C (5% CO_2). Medium was next replaced with RPMI-C supplemented with the vehicle used to dissolve drug (water, methanol or DMSO, to a final concentration of no more than 0.1% v/v). Similar to dose-escalation studies in MPS, new drug was added and allowed to equilibrate to each increasing drug dose over 30 minutes intervals at 37°C, 5% CO_2. After equilibrating monolayers to vehicle and to each dose of drug, spontaneous beating physiology, calcium flux and action potentials were collected in bright-field, GCaMP and BeRST-1 channels, respectively. Next, cells were paced at 1Hz to collect these same three parameters.

Gene Expression in Monolayer Culture.

To characterize gene expression during hiPSC-SC differentiation, cells at various stages of differentiation of hiPSC to endothelial cells were trypsinized, pelleted and lysed (Qiagen RLT lysis buffer supplemented with 1% β-Mercaptoethanol. RNA was recovered using spin columns (Qiagen MicroRNAeasy® kit), with on-column DNAse I digest performed according to the manufacturer's protocol. Purified hiPSC-CM were plated to a density of 200,000 cells/cm^2 on Matrigel coated plates in RPMI-C containing 10μM Y27632. One day after plating medium was exchanged for RPMI-C. Two days following this, monolayers had recovered spontaneous beating, and cells were treated for ten days with either Standard Media (SM) or Maturation Media (MM). Media was exchanged every 3 days. On day 10, cells were washed with PBS and RNA was recovered in the same manner as for monolayer hiPSC-SC. Following RNA recovery from 2D cultures, 500ng of recovered RNA was used to produce cDNA using the SuperScript III kit with Oligo-dT primers (Life Technologies). The obtained cDNA was used to perform SYBR Green and Taqman real-time PCR analysis with the probes described in Supplemental Tables S3 and S4. Commercial polyA-RNA obtained from 15 pooled male/female Caucasians adult human left ventricle (Clonetech, Mountain View, CA) was used as a positive control for expression of cardiomyocyte ion channels, as described previously by Liang[13].

Gene Expression in MPS.

Purified hiPSC-CM were combined with expanded hiPSC-SC as described above for initial optimization studies and cultured for ten days in either standard SM or MM. We first optimized protocols for isolating high-quality (R.I.N. > 8.5) RNA from MPS (data not shown). RNA was extracted from tissue using methods similar to those previously applied for macroscale engineered heart muscle preparations[20]. Briefly, on day 10, MPS were flushed for 10 minutes with PBS at 25°C. Following this wash, MPS were carefully cut with a sterile scalpel, to separate the cell culture chamber from the cell loading chamber of the MPS, and to open the device. The PDMS component, with microtissue attached, was transferred to a microcentrifuge tube, and pooled with up to six other microtissues in lysis buffer from the RNAqueous kit (Thermo). Immediately after adding the tissues to lysis buffer, the microcentrifuge tube containing them was flash frozen in liquid nitrogen. Next, RNA was retrieved from samples by following manufacturer instructions on the RNAqueous kit, followed by DNAse I digestion (Ambion). The yield and quality of RNA were assessed with Qbit and Bioanalyzer, and with optimized methods, we achieved RNA Integrity Numbers above 9. RNA isolated from MPS was amplified using a SMARTeR stranded Pico Input Total RNA library prep kit (Clonetech). The cDNA library products were then diluted by a factor of 10 into sterile water for direct quantitative PCR analysis of relative gene expression. For qPCR analysis, cDNA libraries were diluted by a factor of ten into RNA grade water so that gene expression would fall within the linear assay range.

Mathematical Modeling.

Time-series of AP and Ca^{2+} flux from MPS paced at 1Hz were inverted to a mathematical model of ion channel activity and calcium dynamics to obtain simulated estimates of channel conductance and calcium handling as described in several of our recent publications[28,74,75]. Briefly, a modified version of a model of an immature stem cell[3] was used to calculate the predicted voltage and calcium dynamics. Parameters of this model, specifically maximal channel conductances, intracellular calcium diffusion terms, and surface to area ratios, were then iteratively perturbed until the error between the measured waveforms and simulated waveforms was minimized. Resulting parameters and produced action potential models were then plotted by group to provide an explanation for mechanistic reasons for changes in action potential. It is known that parameterization of such models based on MPS data is challenging and may yield non-unique results; different channel conductances may results in similar voltage output of the model. This issue is discussed by Jæger in a previous study[74] where a method for identifying undetectable parameters was derived. In the present work we have used an inversion with regularization[75] to handle non-unique solutions.

Statistical Analysis.

Direct comparisons were made by unpaired student's 2-way *t*-test. When comparisons were made across more than two groups, a 1-way ANOVA was first performed to determine global significance before performing post-hoc tests for pairwise differences with the Holm-Sidak method, unless noted otherwise in specific figure captions. All curve fitting was done using GraphPad Prism. IC_{50} and EC_{50} curves were fit to four-parameter models. When

these models yielded ambiguous fits (Fig. 4C,D,F,G), a three-parameter model was used. To analyse the currents and calcium flux parameters generated from model fits of action potential and calcium flux waveforms (Fig. 6), we performed a global 1-way ANOVA analysis followed by post-hoc Tukey tests. Gene expression data were statistically analysed with ClustVis (web tool for clustering multivariate data) and GraphPad Prism. Overall PCR data were plotted on ClustVis to obtain heatmaps of the gene expression for maturation media treated MPS relative to standard media values. The genes within 90% percentile of differential expression were then selected and plotted on GraphPad Prism where an unpaired non-parametric t-test was performed to compare standard media and maturation media values using the Holm-Sidak method. Significance was determined with p-value < 0.05.

Extended Data

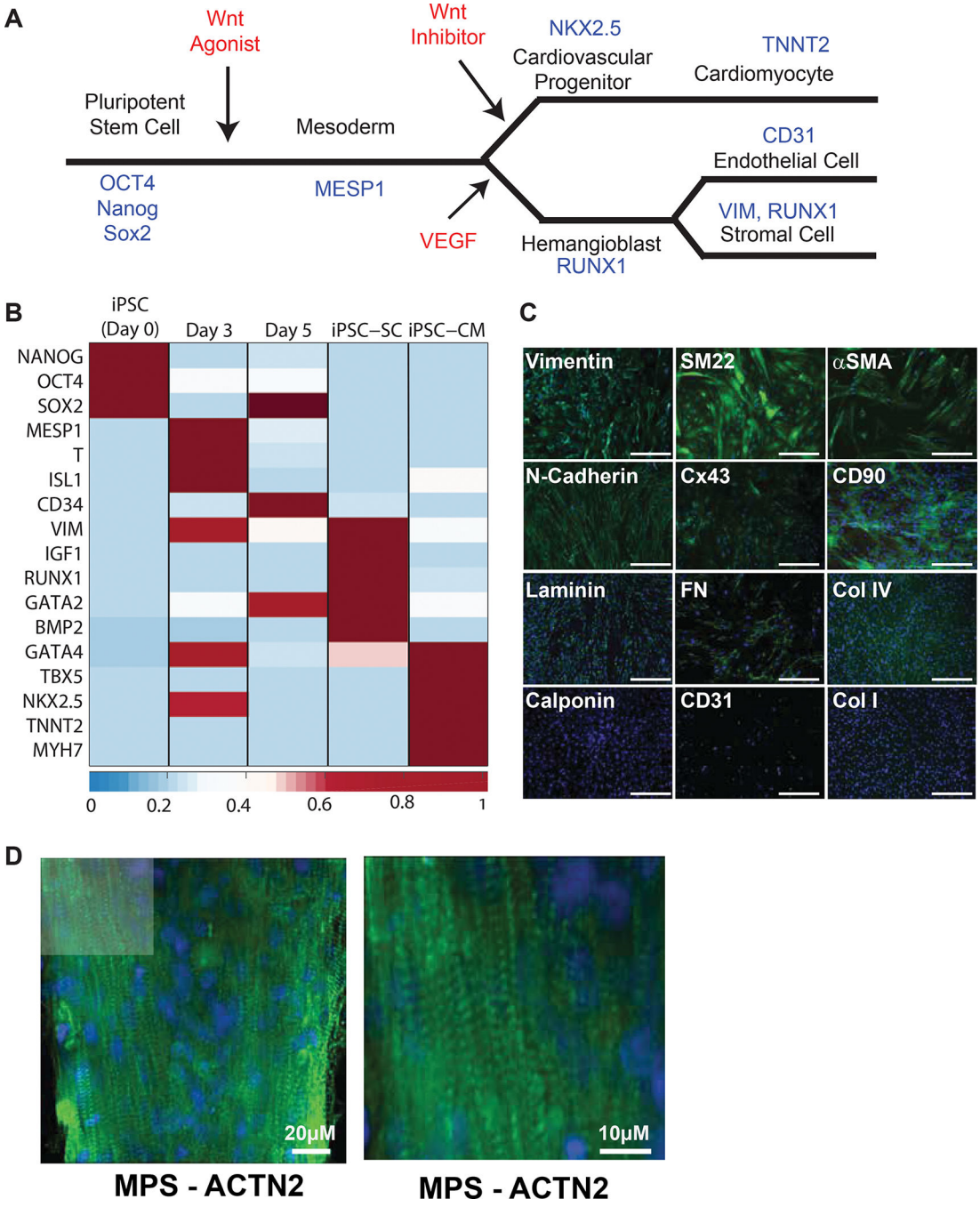

Extended Data Figure 1. Development and Characterization of iPSC-Stromal Cells.

A) Differentiation tree depicting the lineage of iPSC-cardiomyocytes (hiPS-CM) and the isogenic hiPSC-derived stromal cell population (hiPSC-SC). Specific biomarkers (blue) were verified by qRT-PCR. **B)** Brewer plot identifying gene expression patterns over the course of differentiation of hiPSC into hiPSC-SC, with hiPSC-CM included on the plot for comparison. **C)** Immunofluorescence molecular characterization of hiPSC-SC. These

hiPSC-SC were markedly positive for all stromal markers shown, while markers of smooth muscle (Calponin) and endothelial cells (CD31) were not detected. iPS-SC also produce key ECM proteins: Laminin, Fibronectin and Collagen IV, while substantial Collagen I was not detected. **D)** Representative fluorescence micrograph of cardiac MPS, which shows highly organized, aligned cardiomyocytes stained for Sarcomeric α-Actinin (ACTN2, green). Cells were counterstained for nuclei with DAPI (blue) in all fluorescence micrographs. Scale bars: **C**) 500μm **D**) left panel, 20μm and right panel, 10μm.

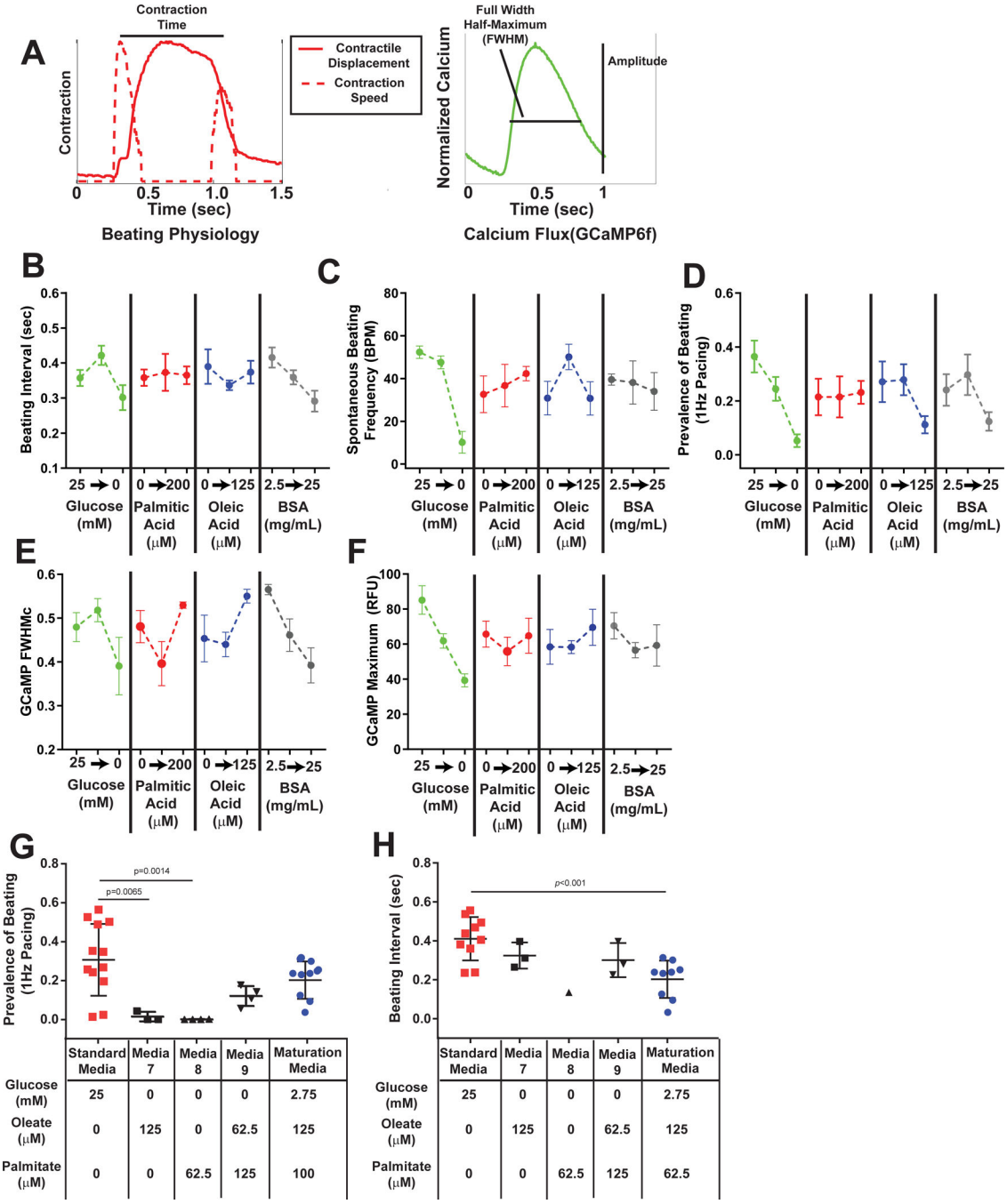

	Standard Media	Media 7	Media 8	Media 9	Maturation Media
Glucose (mM)	25	0	0	0	2.75
Oleate (μM)	0	125	0	62.5	125
Palmitate (μM)	0	0	62.5	125	100

	Standard Media	Media 7	Media 8	Media 9	Maturation Media
Glucose (mM)	25	0	0	0	2.75
Oleate (μM)	0	125	0	62.5	125
Palmitate (μM)	0	0	62.5	125	62.5

Extended Data Figure 2. Design-of-Experiments (DoE) Based Screens Identify Maturation Media for hiPSC-CM Microphysiological Systems.

A) Approach used for initial screen. Computational motion capture is performed on bright-field videos of contracting cardiac MPS, giving the beating interval (defined as the distance between peaks in motion speed for contraction and relaxation, which approximates the interval over which displacement occurs). The knock-in reporter, GCaMP6f, is used to monitor the timing (rate corrected Full-Width-Half-Maximum, FWHM and amplitude of calcium transients in MPS. **B-F)** Results from representative L9 Taguchi Array experiments, depicting **B)** beating interval, **C)** spontaneous beating frequency, and **D)** tissue beating prevalence, all obtained from motion tracking analysis, along with calcium transient **E)** FWHM and **F)** amplitude, obtained from analysis of GCaMP6f fluorescence. Based on 1-way ANOVA tests, glucose levels significantly impact beating interval ($p < 0.05$) along with spontaneous beat rate, beating prevalence at 1hz, and GCaMP amplitude at 1Hz ($p < 0.01$). BSA levels had a significant impact on beating interval ($p<0.05$) and GCaMP FWHM at 1Hz ($p<0.01$). MPS were cultured for ten days prior to analysis for the L9 experiments. **G-H)** Comparison of MPS cultured in standard media (red) to MPS cultured in glucose-free media during L9 studies (black), and MPS cultured in the final Maturation Media (blue) when assessed for (H) beating prevalence at 1hz or (I) beating interval. Data: **B-F**: plot of mean ± SEM, $n = 9$ MPS per group; **H-I**: all data points with mean ± SD, $n = 12$ for SM group, $n = 10$ for MM group, and $n = 3–4$ for all other groups, except for beating interval in media 8, which could only be calculated in $n = 1$ sample (no other samples cultured in this media exhibited either spontaneous or paced beating). p values reflect values obtained from post-hoc Holm Sidak test.

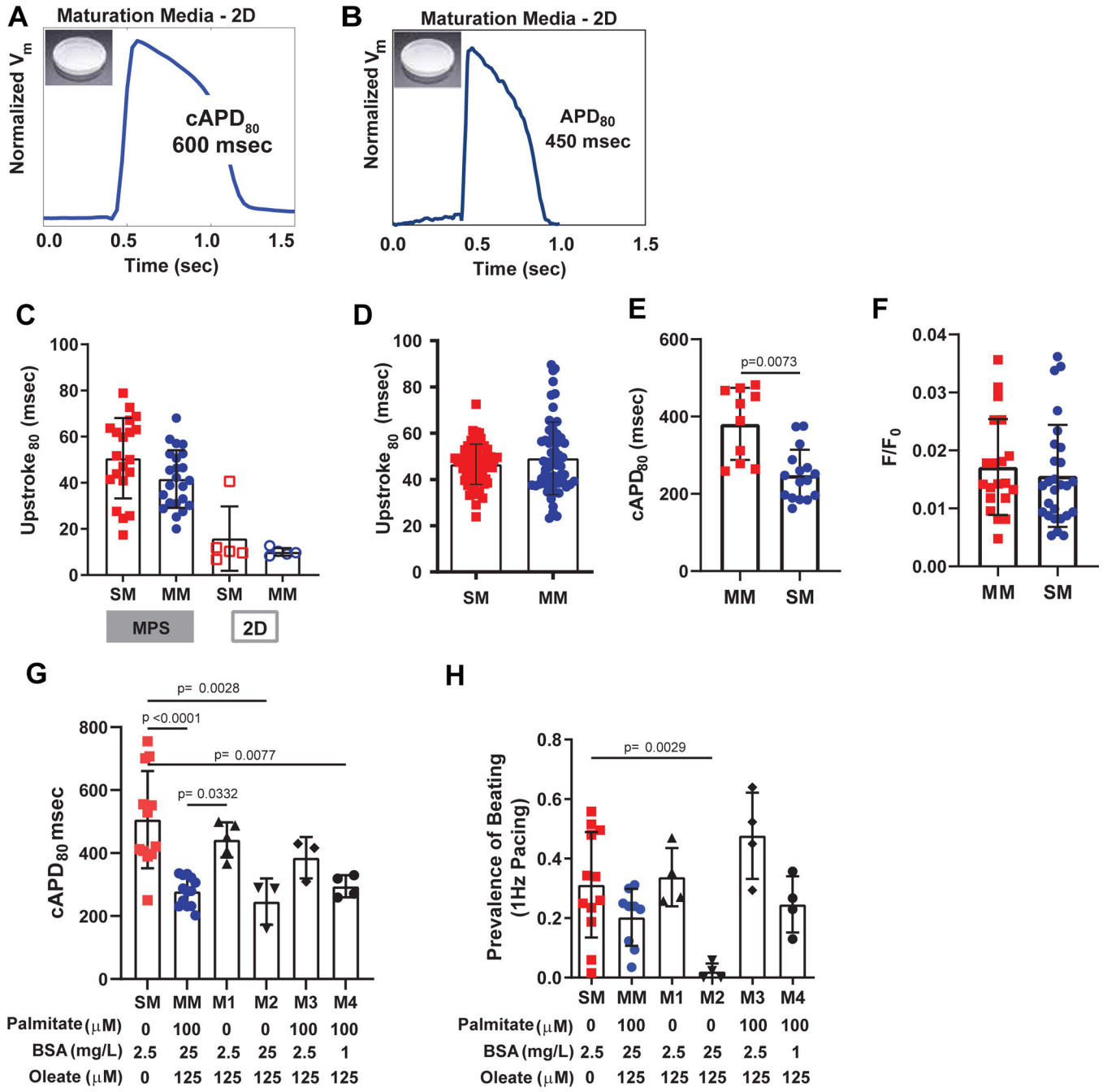

Extended Data Figure 3. Additional information about the media screen and representative 2D traces of MM-treated monolayers.

A-B) Representative action potential tracings for 2D monolayers of **A)** WTC and **B)** SCVI20 cell lines cultured for one week in Maturation Media (MM). **C-D)** Quantification of action potential time from 20% above baseline to peak (Upstroke$_{80}$) in **C)** WTC MPS (n = 5 per group) and 2D monolayers (n = 21 per group) and **D)** SCVI20 MPS (n= 60–63 per group). **E-F)** Quantification of C) beat-rate corrected cAPD$_{80}$ and (MM: n = 16, SM: n = 10 per group); D) background corrected calcium amplitude (F/F$_0$) in SCVI273 MPS (MM: n = 20, SM: n = 25 per group). **G-H)** Analysis of changes in **G)** cAPD$_{80}$ and **H)** contractile

prevalence in MM-pretreated MPS that resulted from modulating the levels of palmitate and albumin in MM. Removing both palmitate and albumin from MM (M1) resulted in MPS with APD80 that were significantly higher than APD80 of MM-treated MPS, and which were no different from APD80 of SM-treated MPS. Removal of Palmitate alone (M2), or of albumin alone (M3) led to a new medium that exhibited APD80 significantly less than MM ($p < 0.05$). Compared to MM, M2 treated MPS exhibited slightly reduced beating prevalence, whereas this metric was enhanced for M3 treated MPS, although these changes were not statistically significant. Slight reduction of the albumin content of MM from 2.5% to 1% (M4) did not have significant effects on APD80 or prevalence of motion in MPS, compared to those treated with MM. All data: plot of all points with median, $n > 5$. (** $p < 0.01$, 2-way t-test with Holm-Bonferonni correction for multiple comparisons).

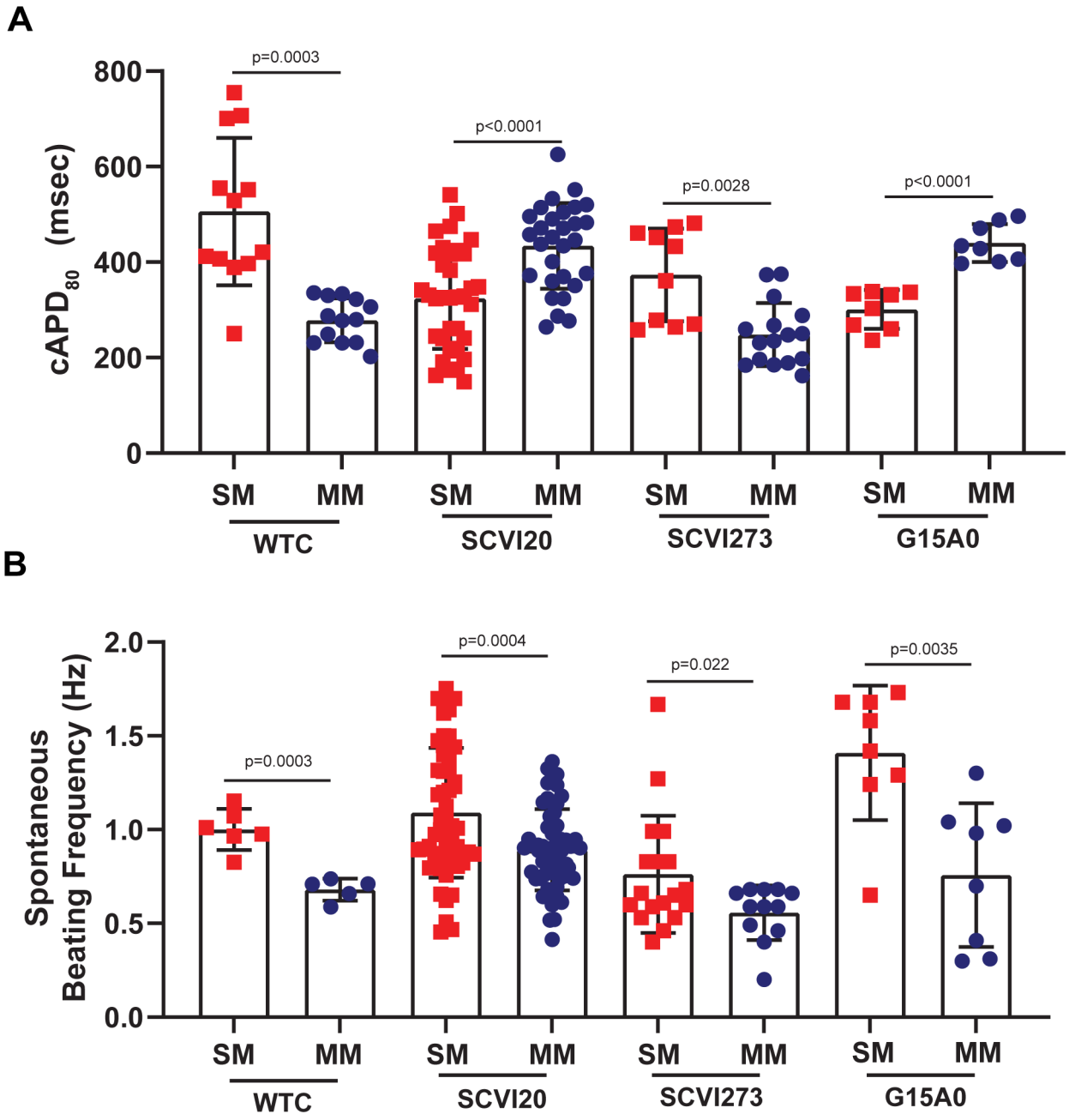

Extended Data Figure 4. Action Potential Duration and Beat Rate in MPS of four genotypes.

A) Randomly selected subset of data on rate-corrected APD_{80} ($cAPD_{80}$) and **B)** Spontaneous beat rate for a representative set of MPS for all four genotypes, pre-treated for 10 days with either SM or MM. *p* values from *t*-test with Welch's correction for non-constant standard deviation.

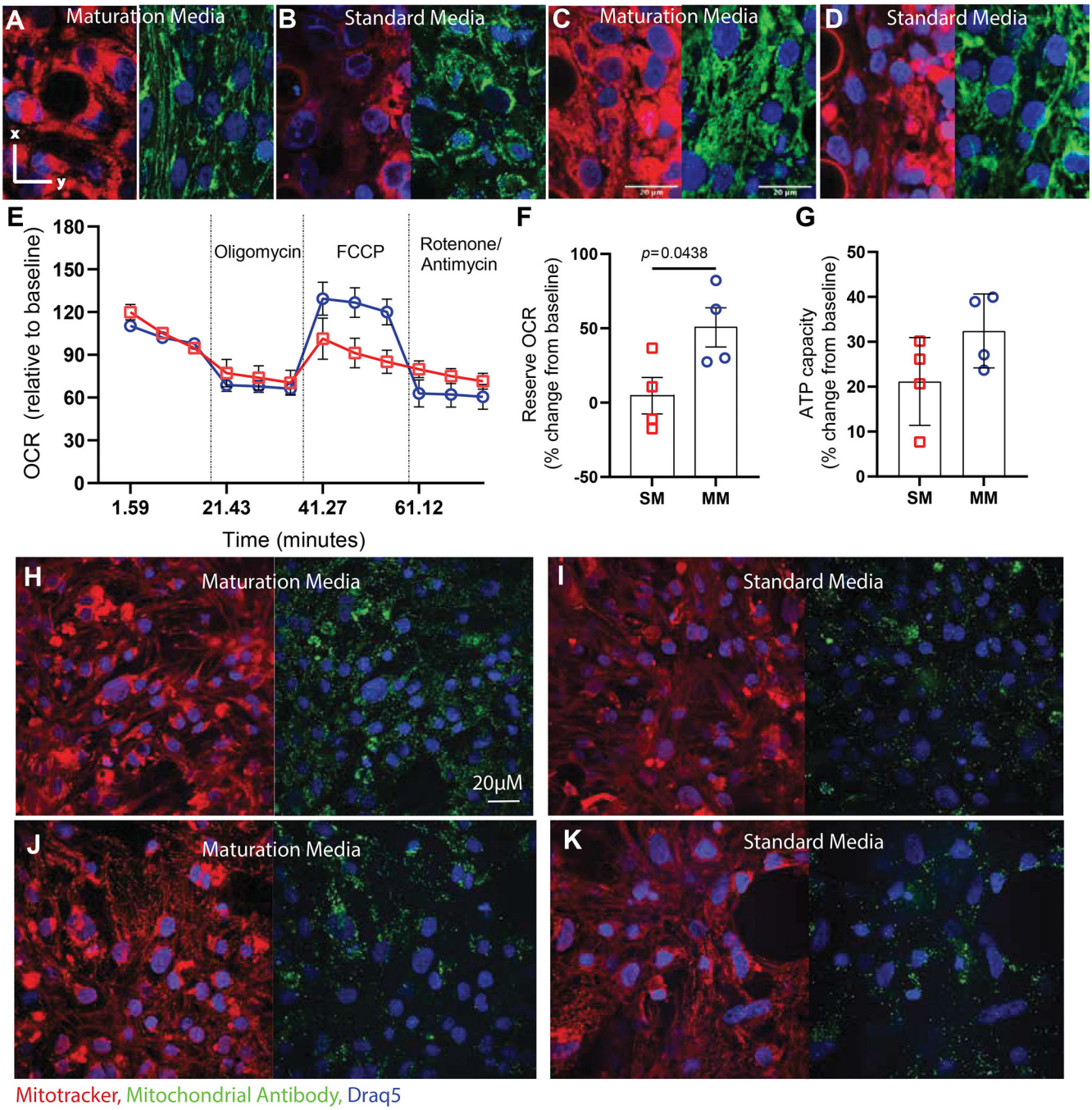

Extended Data Figure 5. Extended Mitochondrial and Metabolic analysis of MPS and 2D iPSC-CM Monolayers.

A-D) Representative images of A-B) SCVI20 and C-D) G15.AO MPS after treatment for 10 days with either (A,C) MM or (B,D) SM. MPS are stained for Mitotracker (red) or anti-mitochondrial antibodies (green) with Draq5 nuclear counterstain (blue). **E)** Representative Oxygen Consumption Rate (OCR) tracings of SCVI20 iPSC-CM monolayers after culture in MM (blue) or SM (red) for 10 days. **F,G)** Quantification of reserve OCR (change in OCR from baseline with FCCP treatment) and total ATP capacity indicate a shift toward

ß-oxidation with MM in 2D monolayers (n = 4 independent wells per group). **H-K)** Representative images of 2D **H,I)** WTC and **J,K)** SCVI20 iPSC-CM monolayers stained with MitoTrackerRed (left; red) and anti-mitochondrial antibodies (right; green). Scale bars: 20μm.

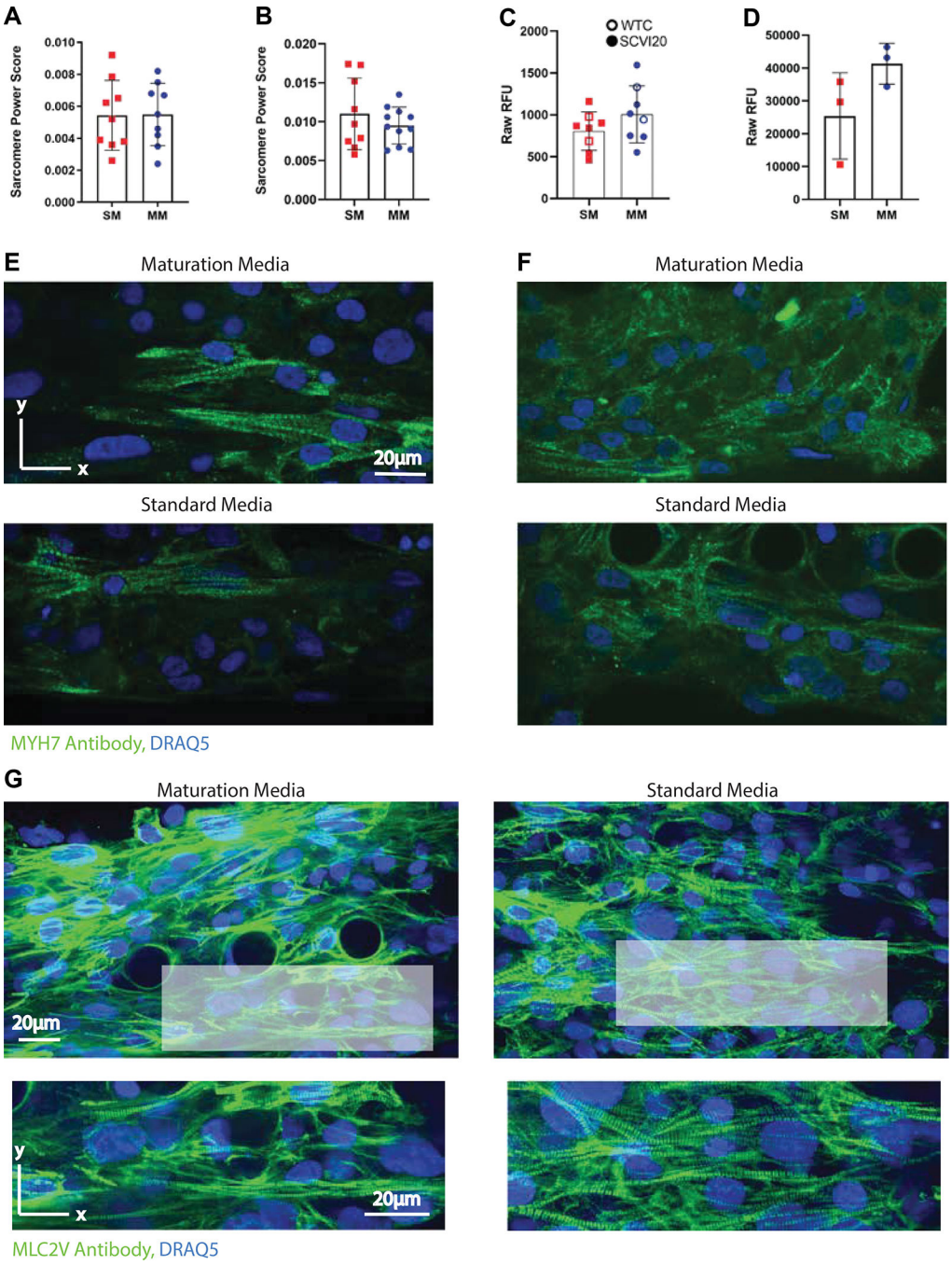

Extended Data Figure 6. Expression and localization of sarcomere proteins in MM-treated MPS. **A-B)** Fourier domain-based quantification of sarcomeric order in MPS treated with SM versus MM for (**A**) WTC or **(B)** SCVI20 cell line treated with MM (blue) or SM

(red) for 10 days (n = 9 independent MPS per group). **C,D)** Quantification of protein expression (antibody staining with analysis by a condition-blinded user) for **C)** MYH7 (n = 8 independent MPS per group; WTC, open squares and circles; SCVI20, closed squares and circles) and **D)** MLC-2v (n = 3 independent MPS per group; SCVI20) in MPS treated for ten days with MM (blue) or SM (red). **E-G)** Representative micrographs of **E)** WTC and **F,G)** SCVI20 MPS after staining for **E,F)** MYH7 and **G)** MLC-2v. Antibody staining in green, with blue Draq5 nuclear counterstain. Scale bars: 20μm.

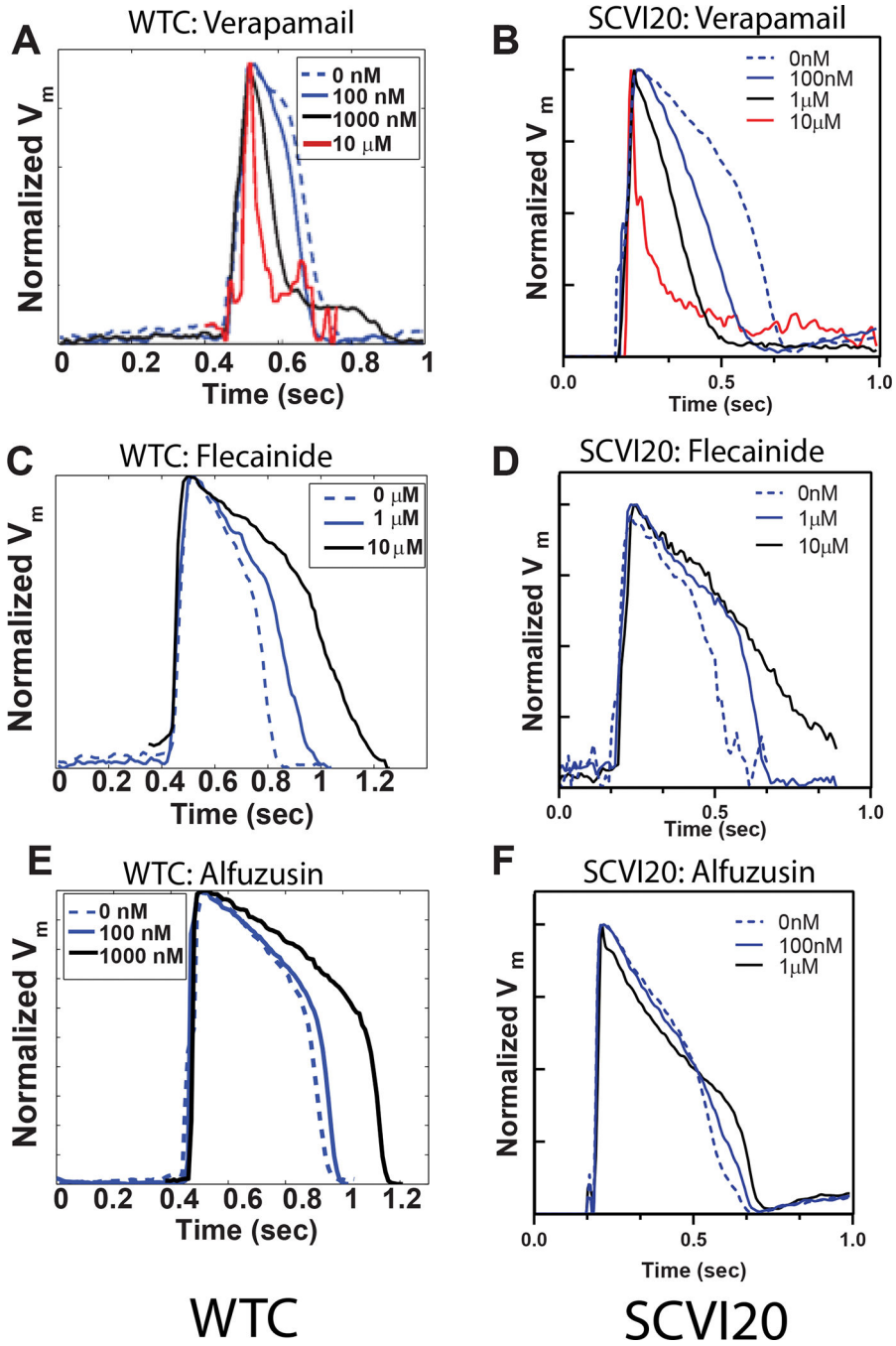

Extended Data Figure 7. Representative action potential changes in MPS exposed to verapamil, flecainide and alfuzosin after MM pre-treatment.

Representative, intensity normalized action potential traces are depicted for (**A,C,E**) WTC and **(B,D,F)** SCVI MPS pre-treated with MM and exposed to escalating doses of (A,B) verapamil, (C,D) flecainide, or (E,F) alfuzosin.

Supplementary Material

Refer to Web version on PubMed Central for supplementary material.

Acknowledgements

This work was funded in part by the California Institute for Regenerative Medicine DISC2–10090 (K.E.H.), NIH-NHLBI HL130417 (K.E.H.), NIH-NIGMS R35GM1195855 (E.W.M.), NIH-NIGMS T32GM066698 (S.B.), the Research Council of Norway INTPART Project 249885, the SUURPh program funded by the Norwegian Ministry of Education and Research, and the Peder Sather Center for Advanced Study (UC Berkeley). We thank Mary West (UC Berkeley) for assistance with image analysis and flow cytometry and Silvio Weber (Technische Universität Dresden) and Stacey Renschler (Washington University in St. Louis) for helpful advice on RNA isolation, cDNA amplification and data analysis. We thank Yoram Rudy, Jeanne Nerbonne, Jon Silva and Jianmin Cui (Washington University in St. Louis) for critical discussions on action potential acquisition, mathematical modeling and data analysis. We thank Bruce Conklin (Gladstone Institutes, San Francisco, USA) for technical advice on the WTC iPSC line, and Joseph Wu (Stanford University) and the Stanford University Cardiovascular BioBank for providing the SCVI20 and SCVI273 iPSC lines and providing technical advice regarding these lines. We thank the Barcelona Stem Cell Institute for providing the G15.AO line.

Professors Kevin E. Healy, Andrew Edwards and Nathaniel Huebsch as well as Sam Wall, Brian Siemons and Verena Charwat have a financial relationship with Organos Inc. and both they and the company may benefit from commercialization of the results of this research.

Data availability

The main data supporting the results in this study are available within the paper and its Supplementary Information. Source data for the figures are provided with this paper. Additional data is available up request.

References

1. Scannell JW, Blanckley A, Boldon H & Warrington B Diagnosing the decline in pharmaceutical R&D efficiency. Nature Reviews Drug Discovery 11, 191–200, doi:10.1038/nrd3681 (2012). [PubMed: 22378269]
2. Musunuru K et al. Induced Pluripotent Stem Cells for Cardiovascular Disease Modeling and Precision Medicine: A Scientific Statement From the American Heart Association. Vol. 11 (2018).
3. Paci M, Hyttinen J, Rodriguez B & Severi S Human induced pluripotent stem cell-derived versus adult cardiomyocytes: An in silico electrophysiological study on effects of ionic current block. British Journal of Pharmacology 172, 5147–5160, doi:10.1111/bph.13282 (2015). [PubMed: 26276951]
4. Johnson EK et al. Differential Expression and Remodeling of Transient Outward Potassium Currents in Human Left Ventricles. Circulation. Arrhythmia and electrophysiology 11, e005914–e005914, doi:10.1161/CIRCEP.117.005914 (2018). [PubMed: 29311162]
5. Kuppusamy KT et al. Let-7 family of microRNA is required for maturation and adult-like metabolism in stem cell-derived cardiomyocytes. Proceedings of the National Academy of Sciences 112, E2785–E2794, doi:10.1073/pnas.1424042112 (2015).
6. Lundy SD, Zhu WZ, Regnier M & Laflamme MA Structural and functional maturation of cardiomyocytes derived from human pluripotent stem cells. Stem Cells Dev 22, 1991–2002, doi:10.1089/scd.2012.0490 (2013). [PubMed: 23461462]

7. Mills RJ et al. Functional screening in human cardiac organoids reveals a metabolic mechanism for cardiomyocyte cell cycle arrest. Proc Natl Acad Sci U S A, E8373–E8381 (2017).
8. Zhang J et al. Functional cardiomyocytes derived from human induced pluripotent stem cells. Circulation Research 104, 30–41, doi:10.1161/CIRCRESAHA.108.192237 (2009).
9. Iseoka H et al. Pivotal Role of Non-cardiomyocytes in Electromechanical and Therapeutic Potential of Induced Pluripotent Stem Cell-Derived Engineered Cardiac Tissue. Tissue Eng Part A 24, 287–300, doi:10.1089/ten.TEA.2016.0535 (2018). [PubMed: 28498040]
10. Lemoine MD et al. Human iPSC-derived cardiomyocytes cultured in 3D engineered heart tissue show physiological upstroke velocity and sodium current density. Scientific Reports 7, 1–11, doi:10.1038/s41598-017-05600-w (2017). [PubMed: 28127051]
11. Ma J et al. High purity human-induced pluripotent stem cell-derived cardiomyocytes: electrophysiological properties of action potentials and ionic currents. AJP: Heart and Circulatory Physiology 301, H2006–H2017, doi:10.1152/ajpheart.00694.2011 (2011). [PubMed: 21890694]
12. Spencer CI et al. Calcium transients closely reflect prolonged action potentials in iPSC models of inherited cardiac arrhythmia. Stem Cell Reports 3, 269–281, doi:10.1016/j.stemcr.2014.06.003 (2014). [PubMed: 25254341]
13. Liang P et al. Drug screening using a library of human induced pluripotent stem cell-derived cardiomyocytes reveals disease-specific patterns of cardiotoxicity. Circulation 127, 1677–1691, doi:10.1161/CIRCULATIONAHA.113.001883 (2013). [PubMed: 23519760]
14. Shadrin IY et al. Cardiopatch platform enables maturation and scale-up of human pluripotent stem cell-derived engineered heart tissues. Nature Communications 8, doi:10.1038/s41467-017-01946-x (2017).
15. Huebsch N et al. Miniaturized iPS-Cell-Derived Cardiac Muscles for Physiologically Relevant Drug Response Analyses. Scientific Reports 6, 1–12, doi:10.1038/srep24726 (2016). [PubMed: 28442746]
16. Mannhardt I et al. Human Engineered Heart Tissue: Analysis of Contractile Force. Stem Cell Reports 7, 29–42, doi:10.1016/j.stemcr.2016.04.011 (2016). [PubMed: 27211213]
17. Godier-Furnémont AFG et al. Physiologic force-frequency response in engineered heart muscle by electromechanical stimulation. Biomaterials 60, 82–91, doi:10.1016/j.biomaterials.2015.03.055 (2015). [PubMed: 25985155]
18. Hinson JT et al. Titin mutations in iPS cells define sarcomere insufficiency as a cause of dilated cardiomyopathy. Science 349, 982–986, doi:10.1126/science.aaa5458 (2015). [PubMed: 26315439]
19. Zhang D et al. Tissue-engineered cardiac patch for advanced functional maturation of human ESC-derived cardiomyocytes. Biomaterials 34, 5813–5820, doi:10.1016/j.biomaterials.2013.04.026 (2013). [PubMed: 23642535]
20. Nunes SS et al. Biowire: A platform for maturation of human pluripotent stem cell-derived cardiomyocytes. Nature Methods 10, 781–787, doi:10.1038/nmeth.2524 (2013). [PubMed: 23793239]
21. Tulloch NL et al. Growth of engineered human myocardium with mechanical loading and vascular coculture. Circulation Research 109, 47–59, doi:10.1161/CIRCRESAHA.110.237206 (2011). [PubMed: 21597009]
22. Tiburcy M et al. Terminal differentiation, advanced organotypic maturation, and modeling of hypertrophic growth in engineered heart tissue. Circulation Research 109, 1105–1114, doi:10.1161/CIRCRESAHA.111.251843 (2011). [PubMed: 21921264]
23. Zimmermann WH et al. Tissue Engineering of a Differentiated Cardiac Muscle Construct. Circulation Research 90, 223–230, doi:10.1161/hh0202.103644 (2002). [PubMed: 11834716]
24. Mathur A et al. Human iPSC-based cardiac microphysiological system for drug screening applications. Scientific Reports 5, doi:10.1038/srep08883 (2015).
25. Charrez B et al. Heart Muscle Microphysiological System for Cardiac Liability Prediction of Repurposed COVID-19 Therapeutics. Frontiers in Pharmacology 12, doi:10.3389/fphar.2021.684252 (2021).
26. Charrez B et al. In vitro safety “clinical trial” of the cardiac liability of drug polytherapy. Clin Transl Sci 14, 1155–1165, doi:10.1111/cts.13038 (2021). [PubMed: 33786981]

27. Jæger KH, Charwat V, Wall S, Healy KE & Tveito A Identifying Drug Response by Combining Measurements of the Membrane Potential, the Cytosolic Calcium Concentration, and the Extracellular Potential in Microphysiological Systems. Frontiers in Pharmacology 11, doi:10.3389/fphar.2020.569489 (2021).
28. Tveito A et al. Inversion and computational maturation of drug response using human stem cell derived cardiomyocytes in microphysiological systems. Scientific Reports 8, doi:10.1038/s41598-018-35858-7 (2018).
29. Ronaldson-Bouchard K et al. Advanced maturation of human cardiac tissue grown from pluripotent stem cells. Nature 556, 239–243, doi:10.1038/s41586-018-0016-3 (2018). [PubMed: 29618819]
30. Ruan J-L et al. Mechanical Stress Promotes Maturation of Human Myocardium From Pluripotent Stem Cell-Derived Progenitors. STEM CELLS 33, 2148–2157, doi:10.1002/stem.2036 (2015). [PubMed: 25865043]
31. Feyen DAM et al. Metabolic Maturation Media Improve Physiological Function of Human iPSC-Derived Cardiomyocytes. Cell Rep 32, 107925, doi:10.1016/j.celrep.2020.107925 (2020). [PubMed: 32697997]
32. Kadota S, Pabon L, Reinecke H & Murry CE In Vivo Maturation of Human Induced Pluripotent Stem Cell-Derived Cardiomyocytes in Neonatal and Adult Rat Hearts. Stem Cell Reports 8, 278–289, doi:10.1016/j.stemcr.2016.10.009 (2017). [PubMed: 28065644]
33. Rupert CE & Coulombe KLK IGF1 and NRG1 Enhance Proliferation, Metabolic Maturity, and the Force-Frequency Response in hESC-Derived Engineered Cardiac Tissues. Stem Cells International 2017, doi:10.1155/2017/7648409 (2017).
34. Tiburcy M et al. Defined Engineered Human Myocardium With Advanced Maturation for Applications in Heart Failure Modeling and RepairClinical Perspective. Circulation 135, 1832–1847, doi:10.1161/CIRCULATIONAHA.116.024145 (2017). [PubMed: 28167635]
35. Fong AH et al. Three-Dimensional Adult Cardiac Extracellular Matrix Promotes Maturation of Human Induced Pluripotent Stem Cell-Derived Cardiomyocytes. Tissue Engineering Part A 22, 1016–1025, doi:10.1089/ten.tea.2016.0027 (2016). [PubMed: 27392582]
36. Yang X et al. Tri-iodo-l-thyronine promotes the maturation of human cardiomyocytes-derived from induced pluripotent stem cells. Journal of Molecular and Cellular Cardiology 72, 296–304, doi:10.1016/j.yjmcc.2014.04.005 (2014). [PubMed: 24735830]
37. Lopaschuk GD & Jaswal JS Energy Metabolic Phenotype of the Cardiomyocyte During Development, Differentiation, and Postnatal Maturation. Journal of Cardiovascular Pharmacology 56, 130–140, doi:10.1097/FJC.0b013e3181e74a14 (2010). [PubMed: 20505524]
38. Makinde A-O, Kantor PF & Lopaschuk GD in Molecular and Cellular Effects of Nutrition on Disease Processes (eds Pierce Grant N., Izumi Tohru, Rupp Heinz, & Grynberg Alain) 49–56 (Springer US, 1998).
39. Correia C et al. Distinct carbon sources affect structural and functional maturation of cardiomyocytes derived from human pluripotent stem cells. Sci Rep 7, 8590, doi:10.1038/s41598-017-08713-4 (2017). [PubMed: 28819274]
40. Rana P, Anson B, Engle S & Will Y Characterization of human-induced pluripotent stem cell-derived cardiomyocytes: bioenergetics and utilization in safety screening. Toxicol Sci 130, 117–131, doi:10.1093/toxsci/kfs233 (2012). [PubMed: 22843568]
41. Matsa E et al. Transcriptome Profiling of Patient-Specific Human iPSC-Cardiomyocytes Predicts Individual Drug Safety and Efficacy Responses In Vitro. Cell Stem Cell 19, 311–325, doi:10.1016/j.stem.2016.07.006 (2016). [PubMed: 27545504]
42. Huebsch N et al. Automated Video-Based Analysis of Contractility and Calcium Flux in Human-Induced Pluripotent Stem Cell-Derived Cardiomyocytes Cultured over Different Spatial Scales. Tissue Engineering Part C: Methods 21, 467–479, doi:10.1089/ten.tec.2014.0283 (2015). [PubMed: 25333967]
43. Sun N et al. Patient-specific induced pluripotent stem cells as a model for familial dilated cardiomyopathy. Science Translational Medicine 4, 130ra147–130ra147, doi:10.1126/scitranslmed.3003552 (2012).

44. Jha AK, Jackson WM & Healy KE Controlling osteogenic stem cell differentiation via soft bioinspired hydrogels. PloS one 9, e98640–e98640, doi:10.1371/journal.pone.0098640 (2014). [PubMed: 24937602]
45. Stile RA, Barber TA, Castner DG & Healy KE Sequential robust design methodology and X-ray photoelectron spectroscopy to analyze the grafting of hyaluronic acid to glass substrates. Journal of Biomedical Materials Research 61, 391–398, doi:10.1002/jbm.10154 (2002). [PubMed: 12115464]
46. Taguchi G & Phadke MS in Quality Control, Robust Design, and the Taguchi Method (ed Dehnad Khosrow) 77–96 (Springer US, 1989).
47. Kitani T et al. Human-Induced Pluripotent Stem Cell Model of Trastuzumab-Induced Cardiac Dysfunction in Patients With Breast Cancer. Circulation 139, 2451–2465, doi:10.1161/CIRCULATIONAHA.118.037357 (2019). [PubMed: 30866650]
48. Zapata-Linares N et al. Generation and characterization of human iPSC line generated from mesenchymal stem cells derived from adipose tissue. Stem Cell Res 16, 20–23, doi:10.1016/j.scr.2015.12.002 (2016). [PubMed: 27345779]
49. Naito H et al. Optimizing engineered heart tissue for therapeutic applications as surrogate heart muscle. Circulation 114, 72–78, doi:10.1161/CIRCULATIONAHA.105.001560 (2006).
50. Wang G et al. Modeling the mitochondrial cardiomyopathy of Barth syndrome with induced pluripotent stem cell and heart-on-chip technologies. Nature Medicine 20, 616–623, doi:10.1038/nm.3545 (2014).
51. Naim JO, Ippolito KML, Lanzafame RJ & van Oss CJ The Effect of Molecular Weight and Gel Preparation on Humoral Adjuvancy of Silicone Oils and Silicone Gels. Immunological Investigations 24, 537–547, doi:10.3109/08820139509066849 (1995). [PubMed: 7790047]
52. Park E-J, Lee AY, Park S, Kim J-H & Cho M-H Multiple pathways are involved in palmitic acid-induced toxicity. Food and Chemical Toxicology 67, 26–34, doi:10.1016/j.fct.2014.01.027 (2014). [PubMed: 24486139]
53. Bodi I, Mikala G, Koch SE, Akhter SA & Schwartz A The L-type calcium channel in the heart: the beat goes on. The Journal of Clinical Investigation 115, 3306–3317, doi:10.1172/JCI27167 (2005). [PubMed: 16322774]
54. Liu R et al. Palmitoylation regulates intracellular trafficking of β2 adrenergic receptor/arrestin/phosphodiesterase 4D complexes in cardiomyocytes. PloS one 7, e42658–e42658, doi:10.1371/journal.pone.0042658 (2012). [PubMed: 22912718]
55. Medda L, Monduzzi M & Salis A The molecular motion of bovine serum albumin under physiological conditions is ion specific. Chem Commun (Camb) 51, 6663–6666, doi:10.1039/c5cc01538c (2015). [PubMed: 25782536]
56. Brandenburger M et al. Organotypic slice culture from human adult ventricular myocardium. Cardiovascular Research 93, 50–59, doi:10.1093/cvr/cvr259 (2012). [PubMed: 21972180]
57. Chen T-W et al. Ultrasensitive fluorescent proteins for imaging neuronal activity. Nature 499, 295–295 (2013). [PubMed: 23868258]
58. Paredes RM, Etzler JC, Watts LT, Zheng W & Lechleiter JD Chemical calcium indicators. Methods 46, 143–151, doi:10.1016/j.ymeth.2008.09.025 (2008). [PubMed: 18929663]
59. Mot AI, Liddell JR, White AR & Crouch PJ Circumventing the Crabtree Effect: A method to induce lactate consumption and increase oxidative phosphorylation in cell culture. Int J Biochem Cell Biol 79, 128–138, doi:10.1016/j.biocel.2016.08.029 (2016). [PubMed: 27590850]
60. Anmann T et al. Formation of highly organized intracellular structure and energy metabolism in cardiac muscle cells during postnatal development of rat heart. Biochim Biophys Acta 1837, 1350–1361, doi:10.1016/j.bbabio.2014.03.015 (2014). [PubMed: 24704335]
61. Ma Z et al. Contractile deficits in engineered cardiac microtissues as a result of MYBPC3 deficiency and mechanical overload. Nature Biomedical Engineering, doi:10.1038/s41551-018-0280-4 (2018).
62. Lee JH, Protze SI, Laksman Z, Backx PH & Keller GM Human Pluripotent Stem Cell-Derived Atrial and Ventricular Cardiomyocytes Develop from Distinct Mesoderm Populations. Cell Stem Cell 21, 179–194.e174, doi:10.1016/j.stem.2017.07.003 (2017). [PubMed: 28777944]

63. Zhang JZ et al. A Human iPSC Double-Reporter System Enables Purification of Cardiac Lineage Subpopulations with Distinct Function and Drug Response Profiles. Cell Stem Cell 24, 802–811 e805, doi:10.1016/j.stem.2019.02.015 (2019). [PubMed: 30880024]
64. Campbell KL & Dicke AA Sarcolipin Makes Heat, but Is It Adaptive Thermogenesis? Frontiers in Physiology 9, doi:10.3389/fphys.2018.00714 (2018).
65. Smith WS, Broadbridge R, East JM & Lee AG Sarcolipin uncouples hydrolysis of ATP from accumulation of Ca2+ by the Ca2+-ATPase of skeletal-muscle sarcoplasmic reticulum. Biochemical Journal 361, 277–286, doi:10.1042/bj3610277 (2002). [PubMed: 11772399]
66. Mall S et al. The presence of sarcolipin results in increased heat production by Ca(2+)-ATPase. J Biol Chem 281, 36597–36602, doi:10.1074/jbc.M606869200 (2006). [PubMed: 17018526]
67. Gorski PA, Ceholski DK & Young HS in Membrane Dynamics and Calcium Signaling (ed Krebs Joachim) 77–119 (Springer International Publishing, 2017).
68. Josowitz R et al. Identification and purification of human induced pluripotent stem cell-derived atrial-like cardiomyocytes based on sarcolipin expression. PLoS One 9, e101316, doi:10.1371/journal.pone.0101316 (2014). [PubMed: 25010565]
69. Schwach V et al. A COUP-TFII Human Embryonic Stem Cell Reporter Line to Identify and Select Atrial Cardiomyocytes. Stem Cell Reports 9, 1765–1779, doi:10.1016/j.stemcr.2017.10.024 (2017). [PubMed: 29173897]
70. Venetucci L, Denegri M, Napolitano C & Priori SG Inherited calcium channelopathies in the pathophysiology of arrhythmias. Nature Reviews Cardiology 9, 561–575, doi:10.1038/nrcardio.2012.93 (2012). [PubMed: 22733215]
71. Buraei Z & Yang J The Beta-subunit of voltage-gated Ca2+ channels. Physiol Rev 90, 1461–1506, doi:10.1152/physrev.00057.2009 (2010). [PubMed: 20959621]
72. Rees CM et al. The Ca(2+) transient as a feedback sensor controlling cardiomyocyte ionic conductances in mouse populations. Elife 7, doi:10.7554/eLife.36717 (2018).
73. Sarkar AX, Christini DJ & Sobie EA Exploiting mathematical models to illuminate electrophysiological variability between individuals. J Physiol 590, 2555–2567, doi:10.1113/jphysiol.2011.223313 (2012). [PubMed: 22495591]
74. Jaeger KH, Wall S & Tveito A Detecting undetectables: Can conductances of action potential models be changed without appreciable change in the transmembrane potential? Chaos 29, 073102, doi:10.1063/1.5087629 (2019). [PubMed: 31370420]
75. Jaeger KH et al. Improved Computational Identification of Drug Response Using Optical Measurements of Human Stem Cell Derived Cardiomyocytes in Microphysiological Systems. Front Pharmacol 10, 1648, doi:10.3389/fphar.2019.01648 (2019). [PubMed: 32116671]
76. Jæger KH, Wall S & Tveito A, doi:10.1101/2020.06.24.168690 (2020).
77. Eisner DA, Caldwell JL, Kistamas K & Trafford AW Calcium and Excitation-Contraction Coupling in the Heart. Circ Res 121, 181–195, doi:10.1161/CIRCRESAHA.117.310230 (2017). [PubMed: 28684623]
78. Parikh SS et al. Thyroid and Glucocorticoid Hormones Promote Functional T-Tubule Development in Human-Induced Pluripotent Stem Cell-Derived Cardiomyocytes. Circ Res 121, 1323–1330, doi:10.1161/CIRCRESAHA.117.311920 (2017). [PubMed: 28974554]
79. Redfern WS et al. Relationships between preclinical cardiac electrophysiology, clinical QT interval prolongation and torsade de pointes for a broad range of drugs: Evidence for a provisional safety margin in drug development. Cardiovascular Research 58, 32–45, doi:10.1016/S0008-6363(02)00846-5 (2003). [PubMed: 12667944]
80. Navarrete EG et al. Screening drug-induced arrhythmia events using human induced pluripotent stem cell-derived cardiomyocytes and low-impedance microelectrode arrays. Circulation 128, doi:10.1161/CIRCULATIONAHA.112.000570 (2013).
81. Aliot E, Capucci A, Crijns HJ, Goette A & Tamargo J Twenty-five years in the making: flecainide is safe and effective for the management of atrial fibrillation. EP Europace 13, 161–173, doi:10.1093/europace/euq382 (2010). [PubMed: 21138930]
82. Melgari D, Zhang Y, El Harchi A, Dempsey CE & Hancox JC Molecular basis of hERG potassium channel blockade by the class Ic antiarrhythmic flecainide. Journal of Molecular and Cellular Cardiology 86, 42–53, doi:10.1016/j.yjmcc.2015.06.021 (2015). [PubMed: 26159617]

83. Bers DM Excitation-contraction coupling and cardiac contractile force. (Kluwer Academic Publishers, 2001).
84. Watanabe H et al. Flecainide prevents catecholaminergic polymorphic ventricular tachycardia in mice and humans. Nat Med 15, 380–383, doi:10.1038/nm.1942 (2009). [PubMed: 19330009]
85. Hilliard FA et al. Flecainide inhibits arrhythmogenic Ca2+ waves by open state block of ryanodine receptor Ca2+ release channels and reduction of Ca2+ spark mass. J Mol Cell Cardiol 48, 293–301, doi:10.1016/j.yjmcc.2009.10.005 (2010). [PubMed: 19835880]
86. Lacerda AE et al. Alfuzosin Delays Cardiac Repolarization by a Novel Mechanism. Journal of Pharmacology and Experimental Therapeutics 324, 427–433, doi:10.1124/jpet.107.128405 (2007). [PubMed: 17986649]
87. Kanzaki Y et al. Three-Dimensional Architecture of Cardiomyocytes and Connective Tissue in Human Heart Revealed by Scanning Electron Microscopy. Circulation 122, 1973–1974, doi:doi:10.1161/CIRCULATIONAHA.110.979815 (2010). [PubMed: 21060087]
88. Lian X et al. Robust cardiomyocyte differentiation from human pluripotent stem cells via temporal modulation of canonical Wnt signaling. Proceedings of the National Academy of Sciences 109, E1848–E1857, doi:10.1073/pnas.1200250109 (2012).
89. Tohyama S et al. Distinct metabolic flow enables large-scale purification of mouse and human pluripotent stem cell-derived cardiomyocytes. Cell Stem Cell 12, 127–137, doi:10.1016/j.stem.2012.09.013 (2013). [PubMed: 23168164]
90. Lian X et al. Efficient differentiation of human pluripotent stem cells to endothelial progenitors via small-molecule activation of WNT signaling. Stem Cell Reports 3, 804–816, doi:10.1016/j.stemcr.2014.09.005 (2014). [PubMed: 25418725]
91. Komeya M et al. Pumpless microfluidic system driven by hydrostatic pressure induces and maintains mouse spermatogenesis in vitro. Sci Rep 7, 15459, doi:10.1038/s41598-017-15799-3 (2017). [PubMed: 29133858]
92. Linkert M et al. Metadata matters: access to image data in the real world. Journal of Cell Biology 189, 777–782, doi:10.1083/jcb.201004104 (2010). [PubMed: 20513764]
93. Laughner JI, Ng FS, Sulkin MS, Arthur RM & Efimov IR Processing and analysis of cardiac optical mapping data obtained with potentiometric dyes. AJP: Heart and Circulatory Physiology 303, H753–H765, doi:10.1152/ajpheart.00404.2012 (2012). [PubMed: 22821993]
94. Fridericia LS The Duration of Systole in an Electrocardiogram in Normal Humans and in Patients with Heart Disease*. Annals of Noninvasive Electrocardiology 8, 343–351, doi:10.1046/j.1542-474X.2003.08413.x (2003). [PubMed: 14516292]
95. Huang YL, Walker AS & Miller EW A Photostable Silicon Rhodamine Platform for Optical Voltage Sensing. Journal of the American Chemical Society 137, 10767–10776, doi:10.1021/jacs.5b06644 (2015). [PubMed: 26237573]
96. Hough PVC Method and means for recognizing complex patterns US patents, Ser. No. 17,715 6 Claims. (Cl. S40–146.3) (1960).
97. Brunelli R Template Matching Techniques in Computer Vision: Theory and Practice. (Wiley, 2009).
98. Schocken D et al. Comparative analysis of media effects on human induced pluripotent stem cell-derived cardiomyocytes in proarrhythmia risk assessment. J Pharmacol Toxicol Methods 90, 39–47, doi:10.1016/j.vascn.2017.11.002 (2018). [PubMed: 29155283]

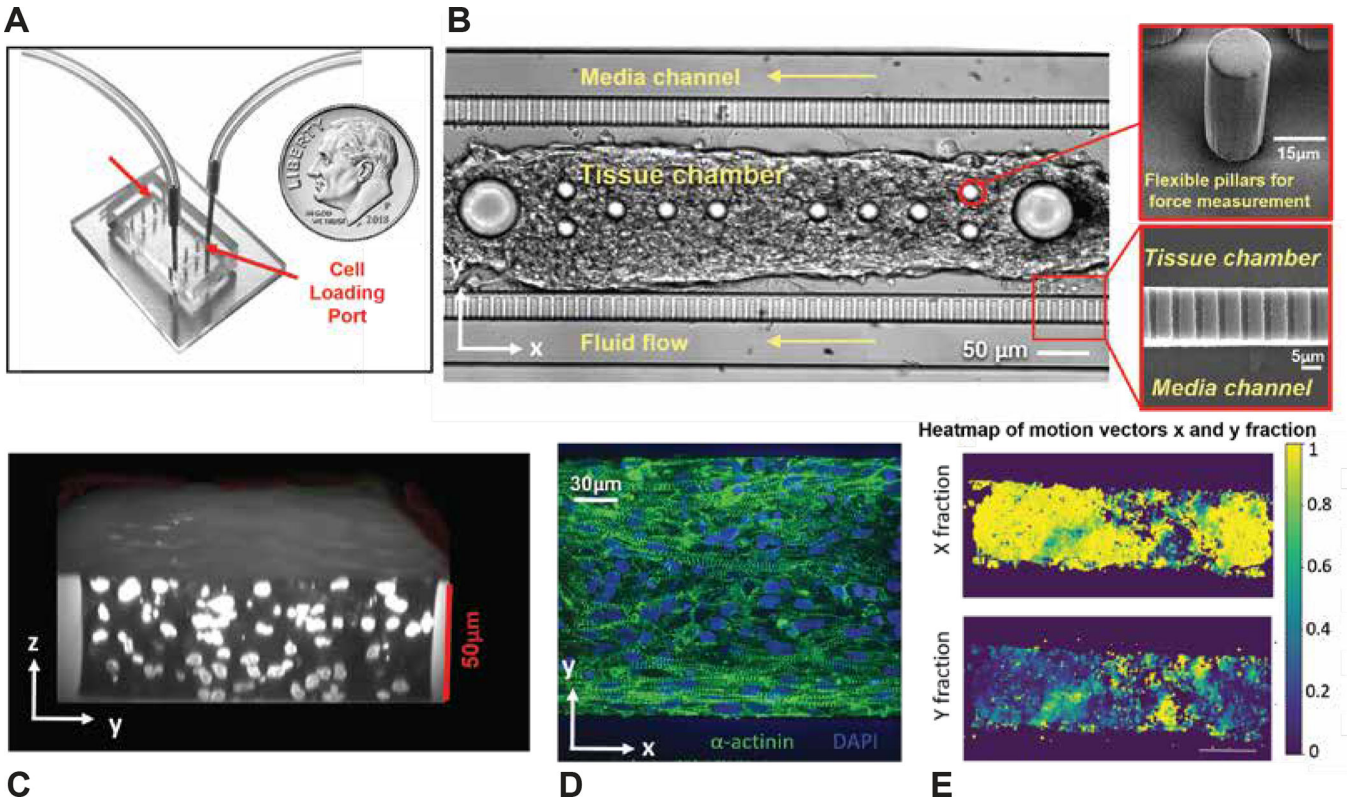

Figure 1. Optimized hiPSC-CM Microphysiological Systems (MPS).

A) Representative image of two cardiac chips parallel to one another. The fluidic inlet and outlet, coupled via tubing, flank the cell loading ports. **B)** Representative brightfield image of a cardiac chip, showing cell loading chamber surrounded by media channels, with accompanying SEM images of flexible pillars for *in situ* contraction force measurements (inset top), and fenestrations insuring diffusive transport of nutrients (inset bottom). **C)** Representative confocal micrograph depicting several layers of cell thickness (side view of DRAQ5 stained nuclei). **D)** Representative confocal micrograph of a cardiac MPS indicating robust sarcomere alignment (sarcomeric α-Actinin, green) and **C)** Heatmap of motion vectors obtained through motion tracking of 8×8 pixel macroblocks overtime. Both length (X) and width (Y) direction of motion vectors are shown, indicating that 95% of the contraction coincides with the orientation of the X axis. These motion vectors were used to analyse the prevalence of beating (centre; percent of the tissue that moves with average speed above a defined threshold that was held constant for all tissues).

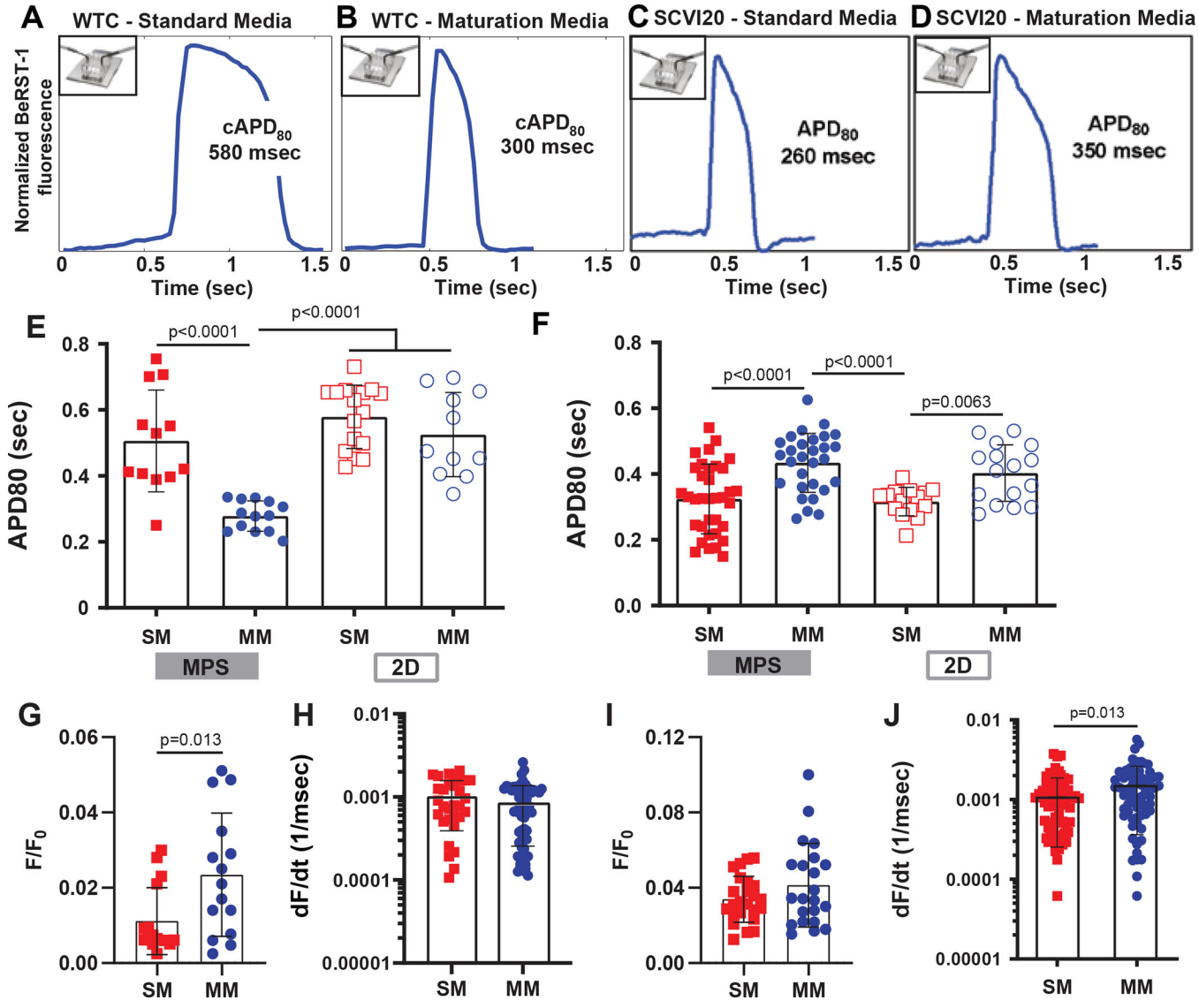

Figure 2. Action Potential Characterization of Matured Cardiac MPS.

A-D) Representative voltage tracings for **(A,B)** WTC MPS and (**C,D)** SCVI20 MPS, cultured for ten days in either (**A,C**) standard cardiac media, or (**B,D**) Maturation Media (MM). **E,F)** Quantitative analysis of 80% action potential duration (APD_{80}) for **E**) WTC (n = 12–16 per group) or **F)** SCVI20 (n = 29–35 per MPS group, n = 15–16 per 2D group) MPS (closed shapes) and monolayers (open shapes), cultured in standard cardiac media (SM; red) or maturation media (blue). **G-J)** Background normalized calcium amplitude of **G**) WTC (n = 15–16 per group) and **I**) SCVI20 (n = 22–24 per group) cell lines, and maximum Ca^{2+} upstroke velocity of **H)** WTC (MM: n = 43, SM: n = 33 per group) and **J**) SCVI20 lines (n = 67–70 per group). All data: plot of all points (each data point represents a different MPS or well of 2D monolayer) with bars depicting mean and standard deviation.

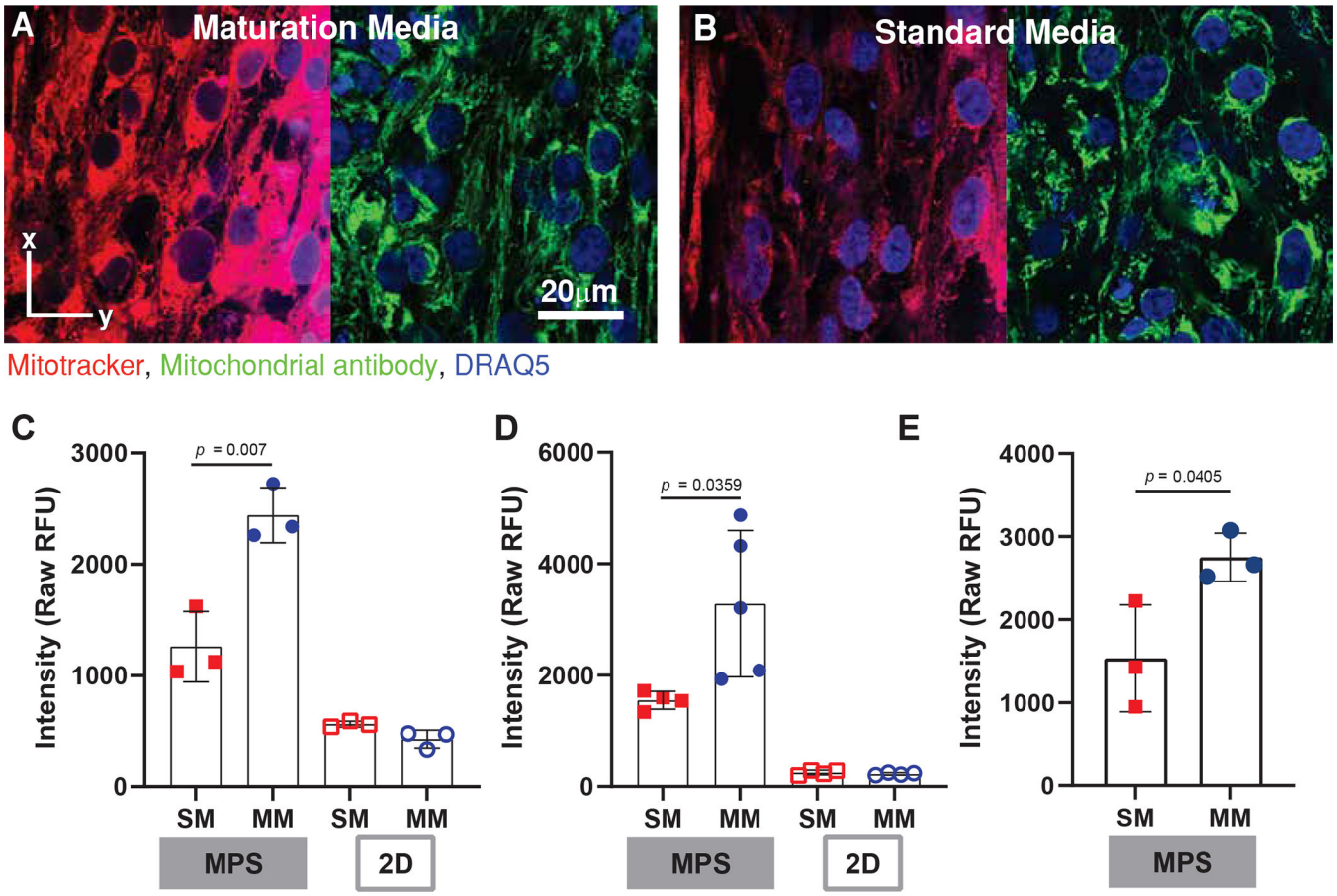

Figure 3. Mitochondrial Morphology of MPS Treated with Maturation Media.

A,B) Representative micrographs of (**A,B**) WTC MPS treated for 10 days with either (**A**) MM or (**B**) SM, then stained with MitoTracker Red (red; left) or anti-mitochondrial antibodies (green; right). Nuclei are counterstained with Draq5 (blue). **C-F)** Quantification of MitoTracker Red intensity in cardiac MPS and 2D monolayers for WTC (n=3 per group) (**E**), SCVI20 (n=4–5 per group) (**F**) or **(G)** G15.AO (n=3 per group). Each data point represents one independent MPS or monolayer well; MPS intensity values of each biological replicate were calculated by averaging five randomly selected fields. Bars depict mean and standard deviation.

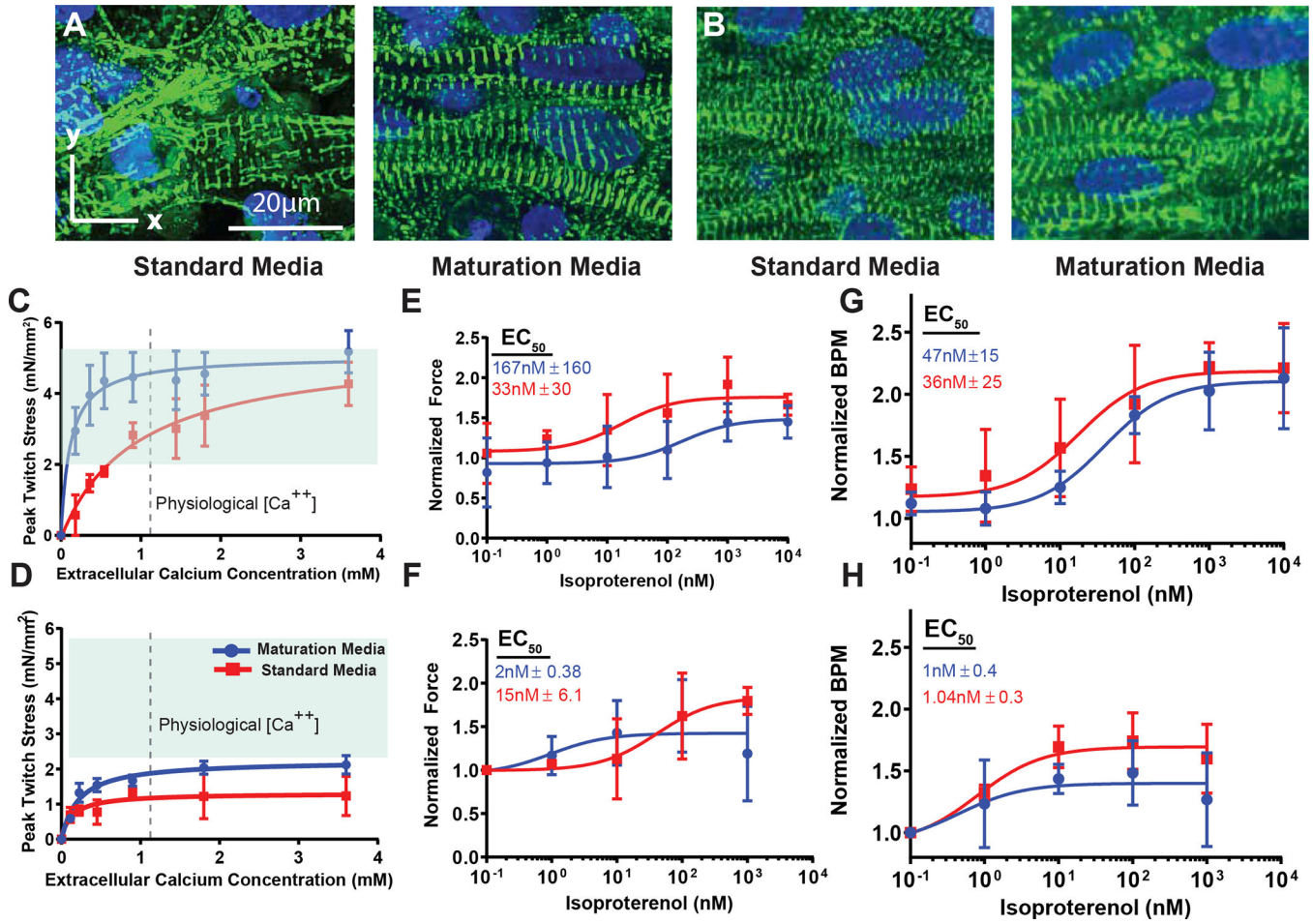

Figure 4. Inotropic Responsive of Maturation Media Treated MPS.

A,B) Representative confocal micrographs depicting sarcomere morphology (Sarcomeric α-Actinin Staining, green, with DAPI nuclear counterstain, blue) of MPS treated for ten days with either standard media (SM) or maturation media (MM) for **A)** WTC and **B)** SCVI20. Contractile stress generated by MPS pre-treated with either SM or MM as a function of extracellular calcium (delivered in Tyrode's saline) for **C)** WTC (n=4 per group) and **D)** SCVI20 (MM: n=7 per group, SM: n=3 per group). The translucent green box denotes the force generated by adult human heart slice cultures[56]. Normalized (**E**) force (n= 4–5 per group) and (**G**) beat-rate (n = 4 per group) as a function of isoproterenol dose in SM and MM pre-treated WTC MPS. Normalized (**F**) force (n= 3–4 per group) and (**H**) beat-rate (n = 4 per group) as a function of isoproterenol dose in SM and MM pre-treated SCVI20 MPS. For force calculation (inotropy), MPS were cultured in Tyrodde's saline with 0.9mM Ca^{2+}. For beat rate calculation (chronotropy), MPS were first equilibrated with to standard media and then received isoproterenol doses in this media. Data are mean ± *SEM*. Scale bars: **A**: left panels, 20μm and right panels, 10μm.

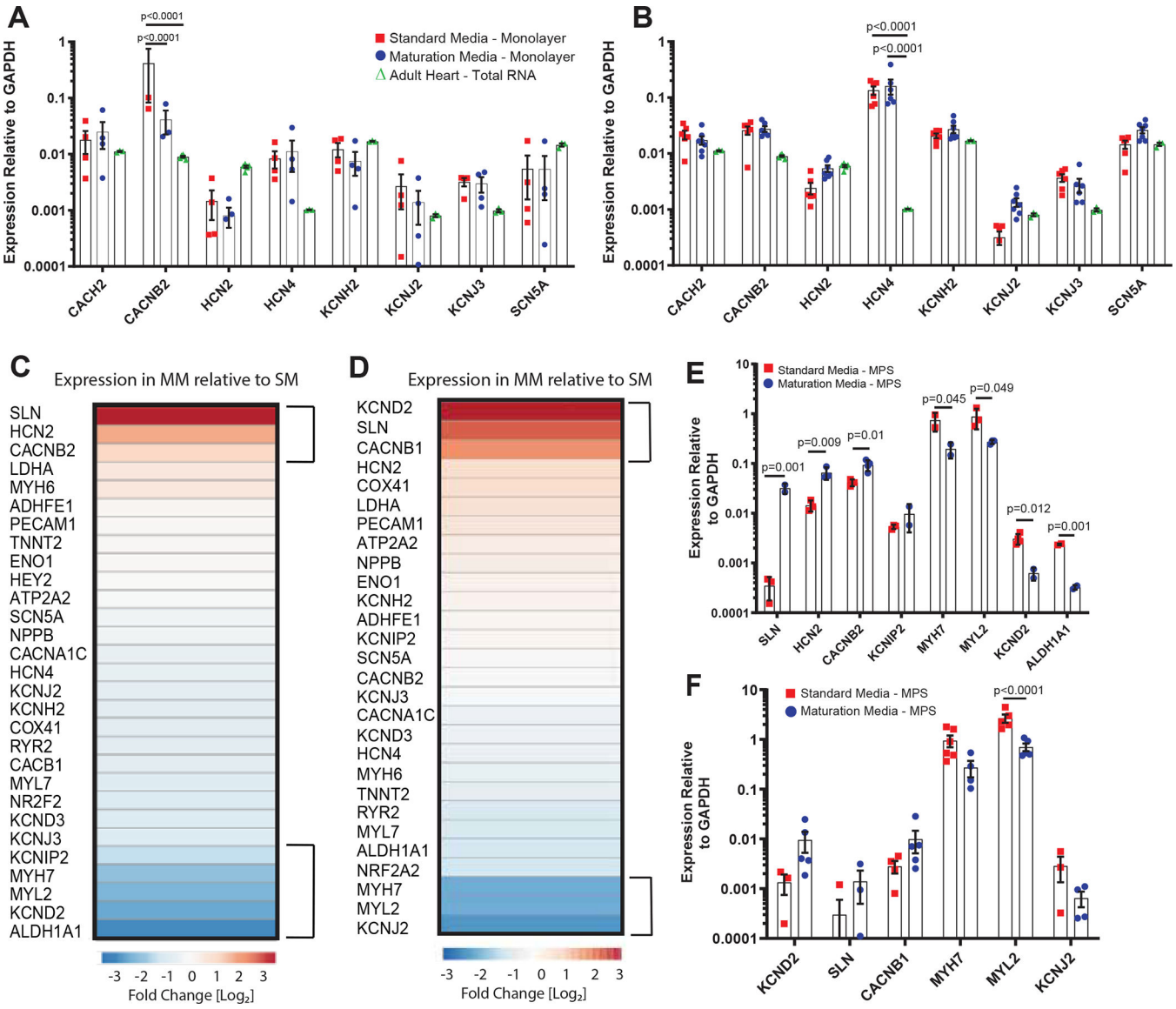

Figure 5. Gene Expression analysis of Monolayers and MPS Treated with Lipid-Based Maturation Media.

Quantitative RT-PCR analysis of expression of ion channel and sarcomere transcripts in hiPSC-CM 2D monolayers after ten days of culture in either Standard (SM; red) or Maturation Media (MM; blue) for **A)** WTC and **B)** SCVI20. None of the genes tested exhibited statistically significant expression changes as a result of Maturation Media. Data: plot of points with median and standard deviation, $n = 4$ wells per condition. Heat-map of relative gene expression in MM-treated MPS as compared to SM-treated MPS, as assessed by qRT-PCR on cDNA libraries amplified from RNA isolated of MPS treated for ten days with SM or MM for **C)** WTC and **D)** SCVI20. Specific analysis for **E)** WTC and **F)** SCVI20, indicating individual biological replicates (treatments of hiPSC-CM obtained from independent differentiations) of differentially expressed transcripts for ion channels or sarcomere genes in MM and SM treated MPS. MPS PCR data were plotted on ClustVis to obtain heatmaps of the gene expression. The genes within 70% percentile of differential

expression were then selected and plotted (**C,D**). Error bars: SEM, $n = 4$ per group (each replicate is a pool of 6–10 individual MPS). p values from 2-way t-test, with Mann-Whitney correction method.

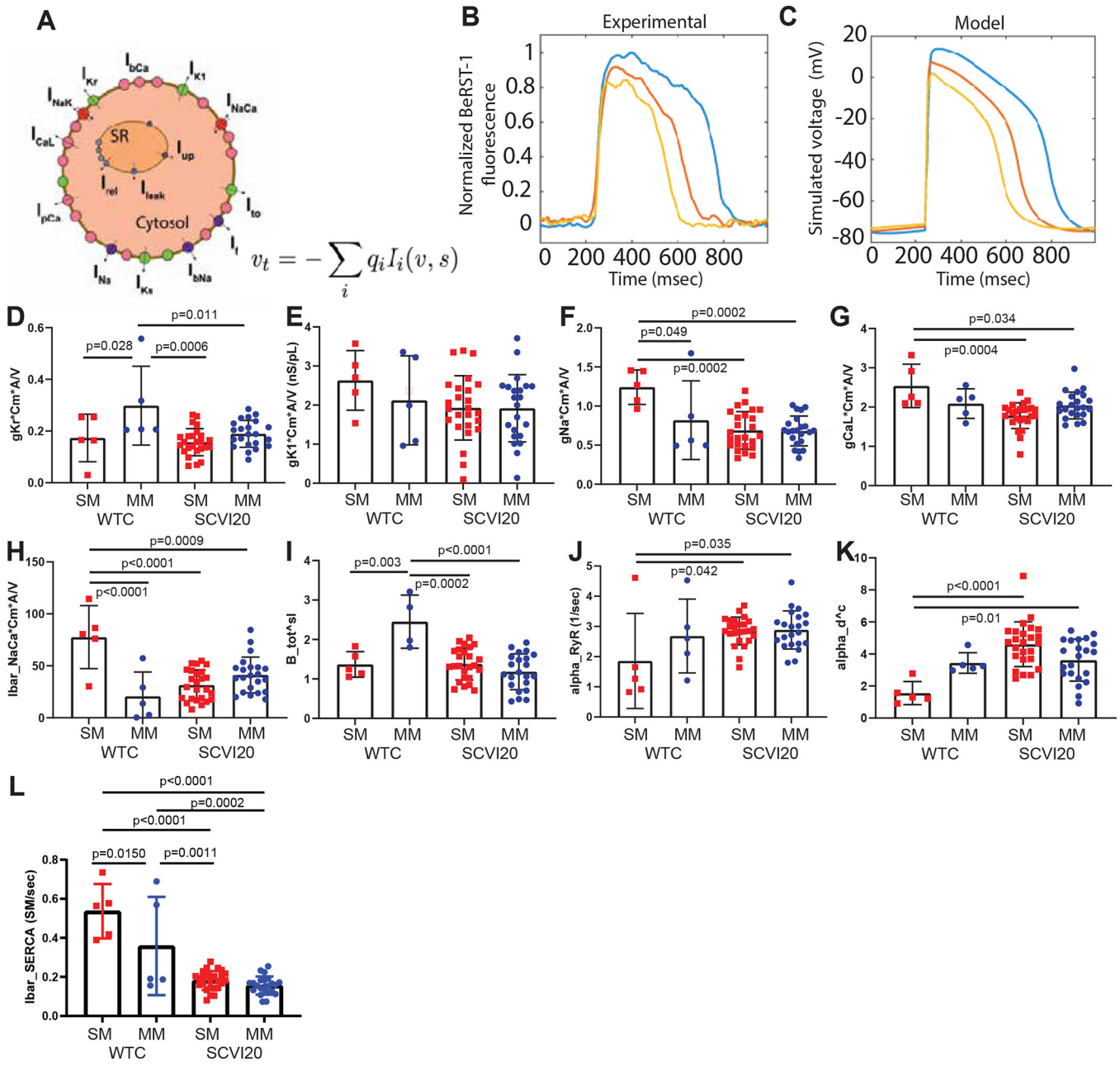

Figure 6. Mathematical Modeling of the Contribution of Individual Currents and Calcium Handling Machinery to the Action Potential of Monolayers and MPS.

A) Schematic of the model. **B)** Examples of experimentally measured action potentials used as model inputs. **C)** Representative simulated action potentials based on the corresponding color of experimentally measured current. **D-G)** Simulated current fluxes. **D-E)** Major potassium currents: D, I_{Kr} (hERG) and E, I_{K1}. **F)** Sodium current, I_{Na}. **G)** *L*-type Calcium current, I_{CaL}. **H)** Sodium-calcium exchange current, I_{NaCax}. **I-L)** Simulated calcium dynamics. **I)** Calcium buffer; **J)** Ryanodine-receptor flux. **K)** Intracellular Ca^{2+} diffusion. **L)** SERCA pump activity. Each data point is the model output from one MPS (n = 4–5 for

WTC, $n = 21$ for SCVI20). p values generated from post-hoc Tukey test following ANOVA across all conditions.

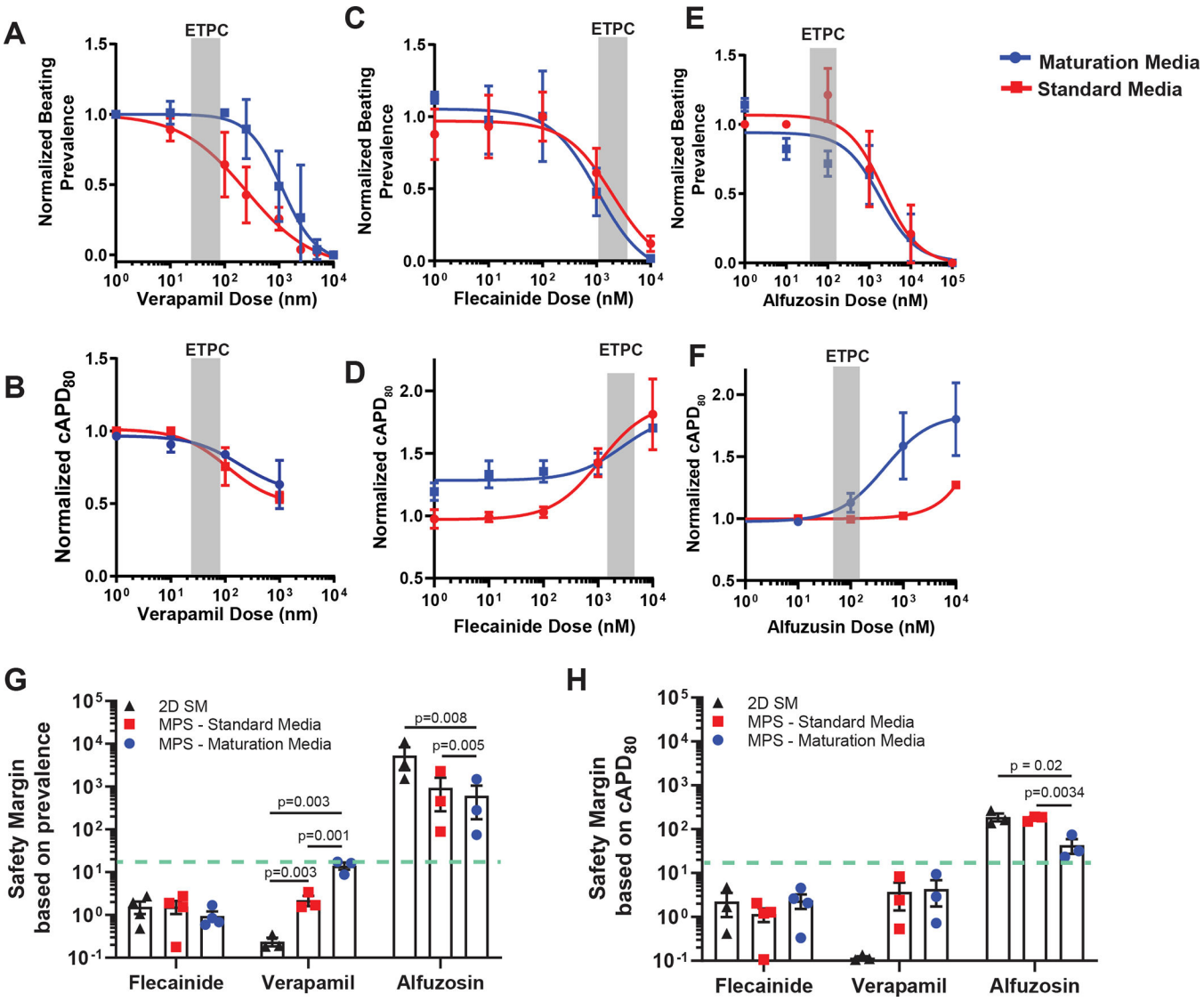

Figure 7. Proarrhythmia Pharmacology of Matured WTC Cardiac MPS.

IC_{50} and EC_{50} analyses were performed in WTC MPS pretreated for ten days with either Maturation Media (blue curves) or Standard Media (Red Curves). For all studies, MPS were equilibrated to Standard Media, and then exposed to escalating doses of **A,B)** Verapamil, **C,D)** Flecainide, or **E,F)** Alfuzosin. IC_{50} curves were obtained by measuring beating prevalence (**A,C,E**) and either IC_{50} or EC_{50} curves by measuring 80% Action Potential Duration (APD_{80}; **B,D,F**). Estimated Therapeutic Plasma Concentration (ETPC) values were obtained from the literature. **G-H)** Safety margins (the ratio of *in vitro* IC_{50} or EC_{50} to literature values for ETPC) calculated based on **G**) beating prevalence and **H**) $cAPD_{80}$. All MPS were paced at 1 Hz for pharmacology analysis. Data: mean ± *SEM*, $n = 4$ individual MPS or well (2D) per group for verapamil studies, $n = 3$ per group for flecainide and alfuzosin studies. p values from 2-way t-test with Holm-Bonferroni correction for multiple comparisons.

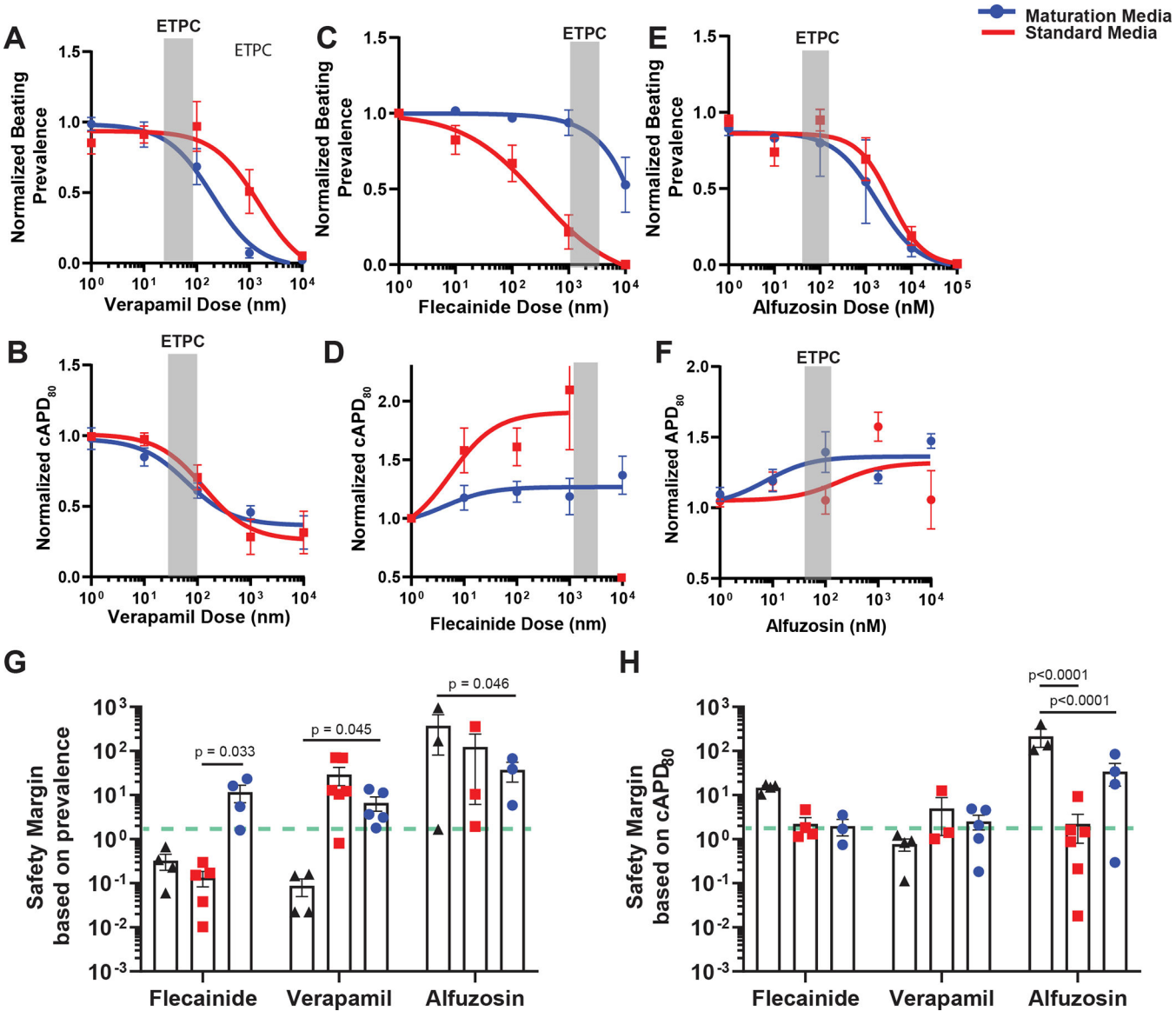

Figure 8. Proarrhythmia Pharmacology of Matured SCVI20 Cardiac MPS.

IC_{50} and EC_{50} analyses were performed in SCVI20 MPS pretreated for ten days with either Maturation Media (blue curves) or Standard Media (Red Curves). For all studies, MPS were equilibrated to Standard Media, and then exposed to escalating doses of **A,B)** Verapamil, **C,D)** Flecainide, or **E,F)** Alfuzosin. IC_{50} of EC_{50} curves were obtained by measuring beating prevalence (**A,D,G**) or 80% Action Potential Duration (APD_{80}; **C,F,I**). Estimated Therapeutic Plasma Concentration (ETPC) values were obtained from the literature. **G,H)** Safety margins (the ratio of *in vitro* IC_{50} or EC_{50} to literature values for ETPC) calculated based on **G**) beating prevalence and **H**) APD_{80}. All MPS were paced at 1 Hz for pharmacology analysis. Data: mean ± *SEM*, n = 3–5 individual MPS or well (2D) per group. p values from 2-way t-test with Holm-Bonferroni correction for multiple comparisons).